Ελληνικό Μεσογειακό Πανεπιστήμιο

Τμήμα Ηλεκτρολόγων Μηχανικών και Μηχανικών Υπολογιστών

Πρόγραμμα Σπουδών Μηχανικών Πληροφορικής ΤΕ

Τίτλος:

Διαφορική και πολυεπίπεδη ανάλυση υφής για την πρόβλεψη της ανταπόκρισης θεραπείας στον καρκίνο του μαστού / Texture Kinetics and Multiscale texture analysis for predicting breast cancer treatment response

Σκεπασιανός Ηρακλής (4083)

Επιβλέπων εκπαιδευτικός : Κωνσταντίνος Μαριάς

Επιτροπή Αξιολόγησης :

- **Κωνσταντίνος Μαριάς**
- **Εμμανουήλ Τσικνάκης**
- **Γεώργιος Παπαδουράκης**

Ημερομηνία παρουσίασης : 8/1/2019

“Texture Kinetics and Multiscale texture extraction based on wavelets for predicting breast cancer treatment response”

Ευχαριστίες

Θα ήθελα να ευχαριστήσω θερμά τον επιβλέπων καθηγητή μου κ. Κωνσταντίνο Μαριά για την καθοδήγηση, βοήθεια και συμβουλές του, που συνέβαλαν στην επιτυχή πορεία της εργασίας αυτής καθώς και στην περαιτέρω ενασχόλησή μου με τον κλάδο της έρευνας. Ευχαριστώ, επίσης, τους υποψήφιους διδάκτορες κ. Κοντοπόδη Ελευθέριο, κ. Βενιανάκη Μαρία και κ. Μανίκη Γεώργιο του εργαστηρίου Υπολογιστικής Βιοιατρικής του Ινστιτούτου Πληροφορικής του Ι.Τ.Ε. για τις ιδέες και συμβουλές που βοήθησαν στην επίλυση προβλημάτων και την βελτίωση της απόδοσής μου στον ερευνητικό κλάδο καθώς και συγγραφής. Τέλος θα ήθελα να ευχαριστήσω το εργαστήριο της Υπολογιστικής Βιοιατρικής για την ευχάριστη ατμόσφαιρα και την βοήθεια.

Abstract

Evaluation of tumor response has been extensively investigated using a wide variety of manual and computer assisted methods. Oncologists are using the Response evaluation criteria in solid tumors (RECIST) and World Health Organization (WHO) criteria, among others, to examine the response of the tumor in the therapy process. However, both of these criteria use the dimensions of the tumor as a feature e.g. its diameter. As a rseult, these approaches are unable to capture the heterogeneity of the tumor tissue structure, which might change after the therapy. For this reason, more accurate quantitative methods for assessing tumor response after therapy have been introduced.

In this work we propose describing breast cancer tissue using texture kinetics and multi-scale texture for the prediction of neoadjuvant chemotherapy response of the patients. As aforementioned, texture features can provide information of the tumor tissue structure in order to overcome current limitations in the RECIST and WHO criteria used in clinical practice. In addition, we propose a framework of Gabor multi-scale filtering to examine the capabilities of multi-scale texture features since texture in different scale provides important information which would be not available in a single scale.

Using a public dataset which includes Dynamic Contrast Enhanced (DCE) Magnetic Resonance Imaging (MRI) data, we examined the texture kinetics and multi-scale textural features, since DCE - MRI provides 3D spatiotemporal evolution of the tumor. More specifically, Radiomic features were extracted, offering a plethora of features describing the tissue heterogeneity of the tumor. Considering that, Radiomic features were examined for analyzing their predictive strength in Neo-adjuvant therapy (NAC) response. Along with this contribution, Radiomic features extracted from Gabor multi-scale filtered images were also extracted in order to address a second research question regarding the role of the scale and orientation of image texture in predicting the therapy outcome.

Results showed that texture kinetics are able to improve the predictability of tumor response to NAC with an area under receiver operating characteristic curve (AUROC) sensitivity of ≈ 81%. Similarly, Gabor multi-scale texture features, provided an average accuracy of >= 70%, while the best accuracy was 88% with scale set at 0.5, confirming that texture at different scales and orientations adds value in the therapy predictive modelling.

Περίληψη

Η αξιολόγηση της ανταπόκρισης του όγκου έχει διερευνηθεί εκτενώς με τη χρήση μιας ευρείας ποικιλίας με χειροκίνητες και με τη βοήθεια υπολογιστή μεθόδους. Οι Ογκολόγοι χρησιμοποιούν, μεταξύ άλλων, τα κριτήρια αξιολόγησης της απόκρισης σε συμπτώματα συμπαγούς όγκου (RECIST) και του Παγκόσμιου Οργανισμού Υγείας (WHO) για να εξετάσουν την ανταπόκριση του όγκου στη θεραπεία. Ωστόσο, και τα δύο αυτά κριτήρια χρησιμοποιούν τις διαστάσεις του όγκου ως χαρακτηριστικό όπως για παράδειγμα τη διάμετρό του. Για αυτό το λόγο, αυτές οι προσεγγίσεις δεν είναι σε θέση να συλλάβουν την ετερογένεια της δομής του όγκου, που μπορεί να αλλάξει μετά τη θεραπεία. Για το λόγο αυτό, έχουν αναπτυχθεί πιο αξιόπιστες ποσοτικές μέθοδοι για την αξιολόγηση της ανταπόκρισης του όγκου μετά τη θεραπεία.

Σε αυτή την εργασία προτείνουμε να περιγράψουμε τον ιστό του καρκίνου του μαστού χρησιμοποιώντας την κινητική της υφής και την υφή πολλών επιπέδων για την πρόβλεψη ανταπόκρισης των ασθενών στην νεο-επικουρική (neoadjuvant) χημειοθεραπεία. Όπως προαναφέρθηκε, τα χαρακτηριστικά της υφής μπορούν να δώσουν πληροφορία για τη δομή του καρκινικού ιστού για να ξεπεραστούν οι περιορισμοί των δημοφιλών κριτηρίων RECIST και WHO. Επιπλέον, προτείνουμε ένα υπολογιστικό πλαίσιο φιλτραρίσματος πολλαπλών επιπέδων Gabor για να εξετάσουμε τις δυνατότητες των χαρακτηριστικών υφής πολλών μεγεθών στην πρόβλεψη του χημειοθεραπευτικού αποτελέσματος.

Με τη χρήση ενός συνόλου δεδομένων που περιλαμβάνει δεδομένα μαγνητικής τομογραφίας με χρήση σκιαγραφικού (DCE- MRI), εξετάσαμε την κινητική της υφής και την υφή πολλών επιπέδων, καθώς η DCE - MRI παρέχει 3D χωροχρονική εξέλιξη του όγκου. Ειδικότερα, εξάχθησαν Radiomic χαρακτηριστικά υφής, τα οποία παρέχουν μια πληθώρα χαρακτηριστικών που περιγράφουν την ετερογένεια του όγκου του όγκου. Στη συνέχεια εξετάστηκαν τα χαρακτηριστικά (Radiomics) ως προς την προγνωστικής τους δύναμη στην πρόβλεψη του αποτελέσματος της νεο-επικουρικής (neoadjuvant) χημειοθεραπείας. Επιεπλέον, τα χαρακτηριστικά Radiomics από τις φιλτραρισμένες εικόνες πολλαπλών κλίμακων του Gabor εξετάστηκαν επίσης και συνέβαλαν σε μια δεύτερη έρευνα, για να διερευνηθεί η σημασία της κλίμακας και κατεύθυνσης της υφής εικόνας στην πρόβλεψη του αποτελέσματος της θεραπείας.

Τα αποτελέσματα έδειξαν ότι η κινητική της υφής είναι ικανή να βελτιώσει την προβλεψιμότητα της ανταπόκρισης του όγκου στην νέο-επικουρική θεραπεία με ευαισθησία ≈ 81% (χαρακτηριστική καμπύλης του δέκτη - AUROC). Παρομοίως, τα χαρακτηριστικά της υφής πολλαπλής κλίμακας Gabor, οδήγησαν σε προβλέψεις με μέση ακρίβεια> = 70%, ενώ η καλύτερη ακρίβεια ήταν 88% με κλίμακα που καθορίστηκε στο 0,5, επιβεβαιώνοντας ότι η ανάλυση υφής σε διαφορετικές κλίμακες και προσανατολισμούς προσδίδει αξία στην πρόβλεψη του θεραπευτικού αποτελέσματος.

Table of Contents

Table of figures

List of tables

1. Introduction

1.1. Breast Tissue

The breast is an organ part of the reproductive system of the human and non-human primates and lies upon the pectoralis major muscle in the upper chest of the body. Both males and females develop this organ and it originates from the same embryological tissues. Breast development starts around the fetal development week 5 and 6 and progresses into puberty. By that time, breast development in female humans is caused by increased growth hormones and estrogens, while androgens in males counteract these effects. Therefore, male humans and other primates significantly less develop their breast, while other female primates usually develop their breasts during pregnancy.

The female breast is responsible for the production of nourishing milk for new-born infants. This is possible by the acini cells; the smallest functional units of the breast, which produce milk in a separate (terminal) duct. Clusters of acini comprise a lobule and numerous lobules comprise a lobe. The ducts are the milk passages that connect the lobules and the nipple. Generally, a normal female breast consists of 15 to 20 lobes. Both ducts and lobules are supported by fat and tissue of the breast. Additionally, a network of ducts increasing in size can eventually form a terminal lactiferous duct where these ducts converge the areola forming the lactiferous sinuses beneath it.

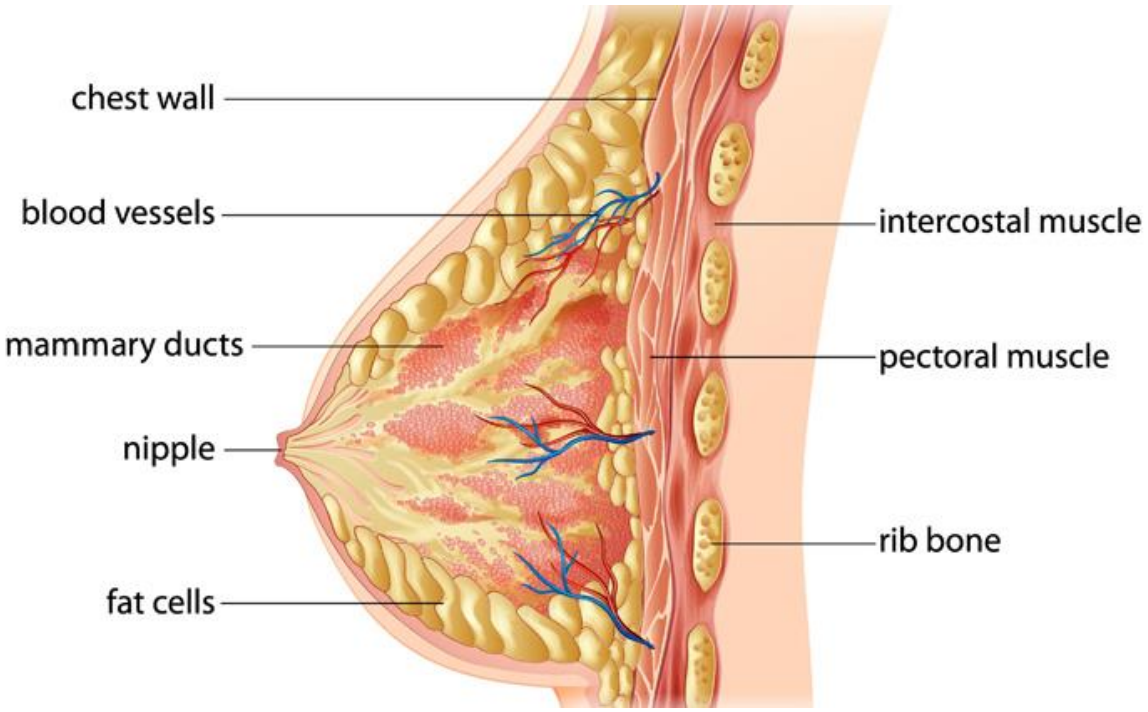

Figure 1: Anatomy of the female breast. Source: breast360.org

1.2. Breast Cancer

Breast cancer is a disease of the breast where cells display an uncontrollable growth in the breast tissue and structure. Early signs of breast cancer are typically a lump which feels different than the rest of the breast. In most cases, breast cancer is discovered after the female human reports feeling a lump in either the breast or the underarm. Other signs of breast cancer may include substantial growth or shrinking of one breast, a nipple changing its shape or position, a rash around the tissue of a nipple and a persistent pain in the breast. Another case is the inflammatory breast cancer which is an aggressive form of breast cancer which can be detected by the swollen areas on the breast. A malignant tumor can result in metastatic tumor, one of breast cancer most important characteristic, in which case, secondary tumors spread in other organs or tissues. While the site of origin is a significant parameter in where the metastasis happens, most common sites include the brain, liver, lung and bone. This invasive state is categorized as stage 4 breast cancer with the rate of survivability dropping to a small percentage.

Besides stage 4, which is the last stage of breast cancer and the most fatal one, there are 4 more stages, starting from stage 0 increasing to 4. A stage 0 breast cancer is the earliest stage of breast cancer and is also called carcinoma in situ. Stage 0 is the stage where the tumor has not spread into other parts of the breast and its often difficult to detect. It is also considered a precancerous condition where no treatment is required, but a close observation is advisable. Two sub-stages can be deducted from this one, named Ductal carcinoma in situ and Lobular carcinoma in situ. A stage 1 breast cancer characterizes the tumor which has not spread beyond the starting location while its size is less than 2 centimeters (cm) while no lymph nodes have been involved. Because of its size, it is difficult to detect it. This stage is split into two sub-stages, stage 1A and stage 1B, where the first characterizes a tumor less of 2cm and no spreading outside the breast, whilst the second includes the spreading of small cancer cells with size of no more than 2 millimeters (mm). The mortality rate of stage 1 breast cancer is 98% to 100% [1]. A stage 2 breast cancer is the stage that the tumor is measured between 2 and 5 cm, or if the cancer has spread into another part of the breast, including the lymph nodes of the underarm. Two sub-stages are also deducted in which stage 2A is when the tumor is not within the breast but in the underarm lymph nodes, or when in it's the breast with a size of 2cm or smaller and it spread into the underarm lymph nodes, or when the tumor size is between 2 and 5 cm with no spreading to the underarm. The second sub-stage is the stage 2B which is when the tumor size is measured between 2 and 5 cm and it has spread to the underarm lymph nodes, or when the size of the tumor is more than 5cm with not spreading to the underarm. The survival rate of stage 2 breast cancer is 90% to 99%. The next stage is the stage 3 which characterizes a tumor of more than 2 cm size in diameter and the extensive spreading in the underarm lymph nodes or other lymph nodes or tissues near the breast. Stage 3 has three sub stages, where stage 3A is when there is no tumor in the breast but in underarm lymph nodes or near the breast bone, when the tumor size is less than 2 cm and has spread to axillary lymph nodes attached to each other or near the breast bone, when tumor size is between 2 and 4 cm and has spread to axillary lymph nodes, or lymph nodes near the breast, or when the tumor size is more than 5cm and it has spread axillary lymph nodes or lymph nodes near the breast bone. Stage 3B is

when the tumor has spread to the chest wall or breast skin and may have spread to underarm lymph nodes or to other structures or to lymph nodes near the breastbone, or when it's characterized as inflammatory breast cancer. Stage 3C is when the tumor has spread to the chest wall or the skin with no presence in the breast, or when its present in lymph nodes close to the collarbone, or when cancer cells have spread to the lymph nodes close the breastbone. A stage 3 cancer can be operable, but inoperable when the cancer has spread to the lymph nodes above the collarbone. The mortality rate of a stage 3 breast cancer is between 66% to 98%. Lastly, stage 4 breast cancer is the metastatic breast cancer meaning the cancer has spread to other parts of the body including bone, brain, lungs or liver. Stage 4 mortality rate is at 35.5%.

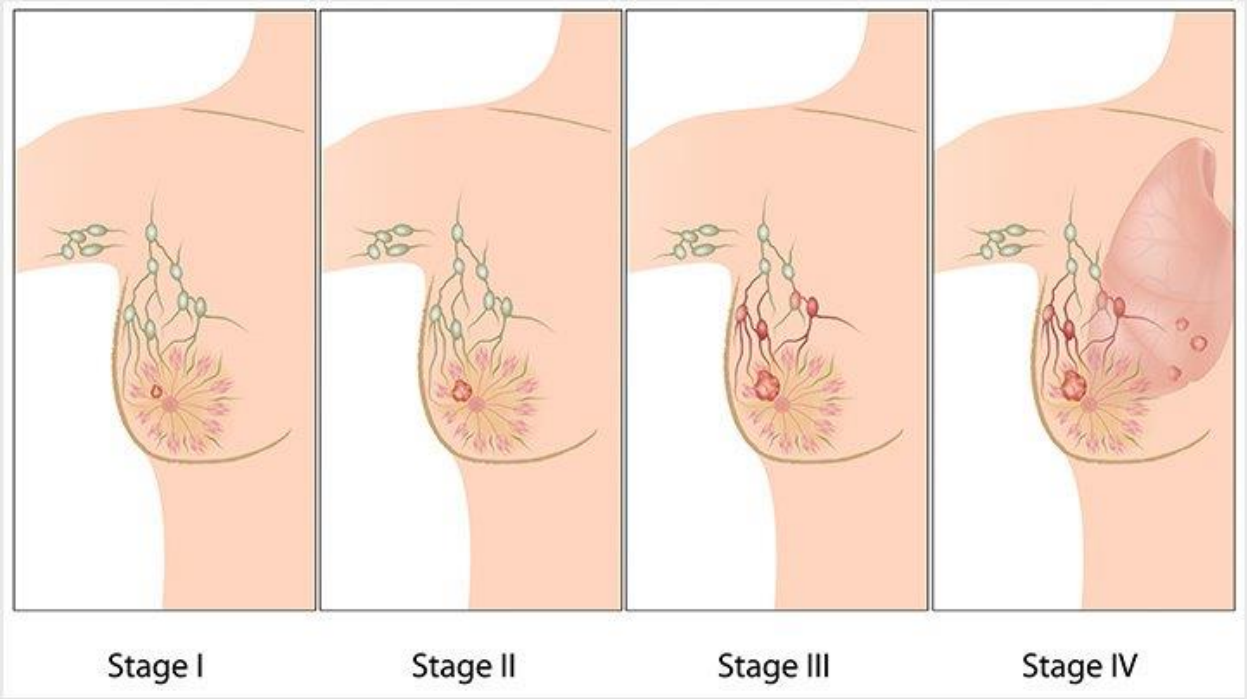

Figure 2: Illustration of breast cancer stages. Source: https://www.everydayhealth.com/breast-cancer/stages-what-they-mean

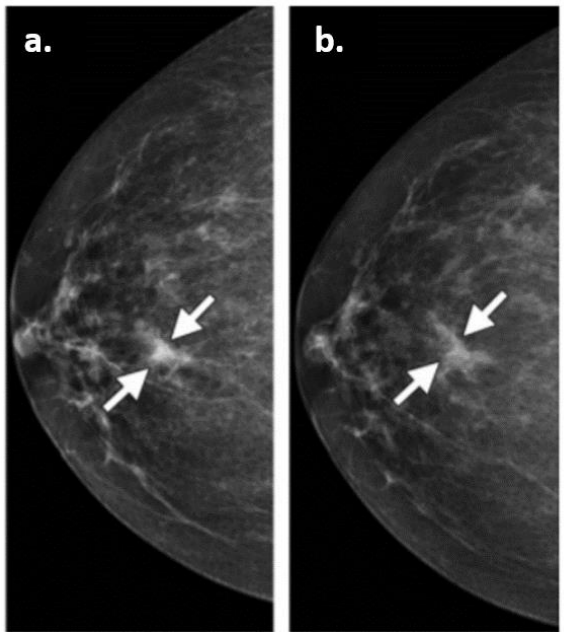

Figure 3: Examples of invasive ductal carcinoma in a female patient.. Source [2]

Breast cancer is the most common aggressive cancer in women, affecting several of them. [3] An estimation of the number of the affected women is 2.1 million patients in the year 2018, with a new case being diagnosed approximately every 18 seconds [4]. Moreover, 600 thousand women have died due to breast cancer. Globally, there is an increase of breast cancer incidents of 3.1% of records beginning in 1980 with 641.000 cases, increasing to more that 1.6 million in 2010. Regardless of any socioeconomic status, the increase of incidents can be related to the increase in total population since 49.5% of the global population is female with the larger proportion being more than 60 years old. Additionally, advanced breast cancer patients’ number is unknown, forcing most countries researchers to prioritize its epidemiology.

Breast cancer is reported to be inherited by 10% of the cases associated with a family history, with first-degree relatives of potential cancer patients having a risk of showing breast cancer before the age of 35. While family history is an important parameter to consider, there has been developed a family history scope to evaluate the chance by considering other factors like environmental, relation degree or family size [5]. Environmental and lifestyle factors are important considering the national awareness campaigns all around the world. With the increase in 1980s and 1990s, screenings and physical examinations have increased, thus increasing the cases and the survivability of the patients since the examinations happen in the early stages of the cancer. Lifestyle factors like first pregnancy in advanced age has also increased the number of cases worldwide, playing a significant role in social and health awareness. Additionally, health factors created by certain lifestyles like obesity, lack of physical activity and alcohol consumption, comprise an approximate 20% of breast cancer beginning cause. As a report stated, an adult woman with a consumption of 10 grams of alcohol daily, will have a 7% to 10% increase in breast cancer risk [6].

Even though, breast cancer mostly affects women, it can be developed in male population as well. Male breast cancer is a rare disease that accounts for less than 1% of all men's cancers and less than 1% of all breast cancers. Lifetime risk of breast cancer in men is 1 in 833 when for women is 1 in 10 [7].

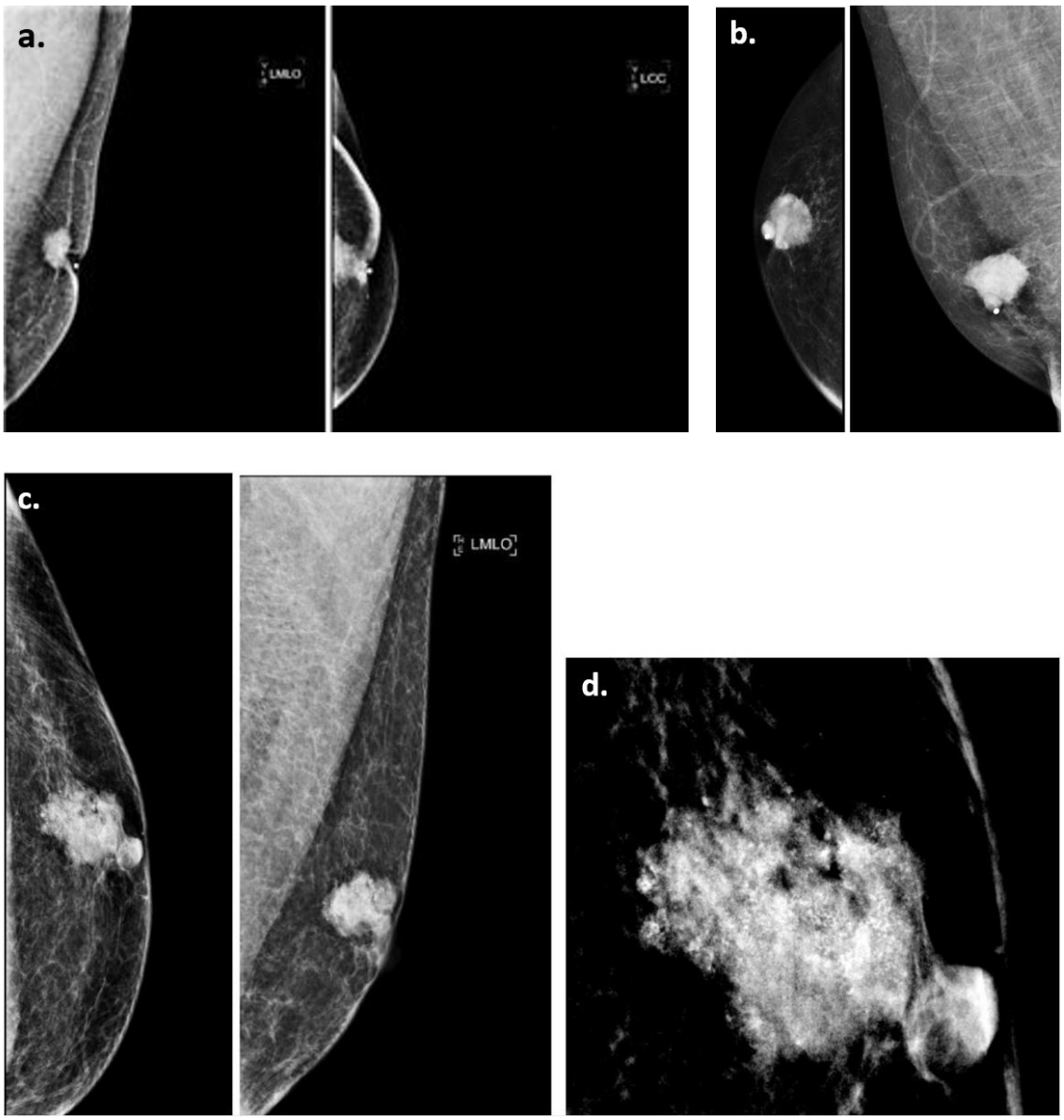

Figure 4: Examples of mammographic appearance of a male breast cancer in a (a) 89-year-old patient with nipple retraction and a (b) 68-year-old patient. In (c) an Invasive ductal carcinoma in a 58-year-old man with palpable mass is illustrated. In (a) and (b) the mammograms show a high density subareolar irregular shaped mass with spiculated borders. In (c) the mammograms depict s high-density mass in the union of the inferior quadrants.

Source:
https://posterng.netkey.at/esr/viewing/index.php?module=viewing_poster&task=viewsection&pi=149371&ti=542912&si=1773&searchkey=

Concerning the factors of breast cancer growth, 20% have a first-degree family history while other factors like increased estrogens, liver cirrhosis, obesity, smoking and prostate cancer still posing a significant addition in risk of developing cancer. Implications of breast cancer in men are present in older age and with higher stage than women of the same situation. Invasive ductal carcinoma is the most common subtype, while invasive lobular carcinoma being rarer compared to female breast cancer. Prognosis is the same with female patients of similar stage, however male patients' survival rate is much less considering the patients' older age, more comorbidities and also lower life expectancy [8], [9]. Therapies for male breast cancer are similar to those of female, with endocrine therapy being the most popular one due to the fact that luminal cancers are the most common cases of male breast cancer. Recommendations for adjuvant chemotherapy and radiation therapy are similar to women, as are recommendations for management of advanced breast cancer [9], [10].

1.3. Breast Cancer Imaging

Breast cancer imaging is achieved by mammography, ultrasound or Magnetic Resonance Imaging (MRI). Recent studies show conflicting results regarding which technique is the most effective in breast cancer imaging. Mammography is the most popular one, however there is a debate ongoing whether mammography is harmful or not to the patient, due to the ionizing radiation dose of X-ray used. Another reason this debate exists is the false-positive lesion characterization that result from mammograms regularly. Additionally, for young women it is suggested to use screening methods of ultrasound and MRI instead of mammography. Furthermore, the combination of this imaging techniques provides a better cancer detection in high breast density, however there is not a clear evaluation of mortality outcome. [21]

More specifically, mammography is an imaging technique which utilizes low-energy X-rays in order to screen the human breast for diagnosis. Mammography's goal is the detection of breast cancer at an early stage. Mammography's popularity increased after 1960, as there was not an existing screening protocol. This includes improvements in sensitive imaging resolution, low x-ray absorption cassettes, dedicated processors and improved films.

Figure 5: A normal breast mammography.

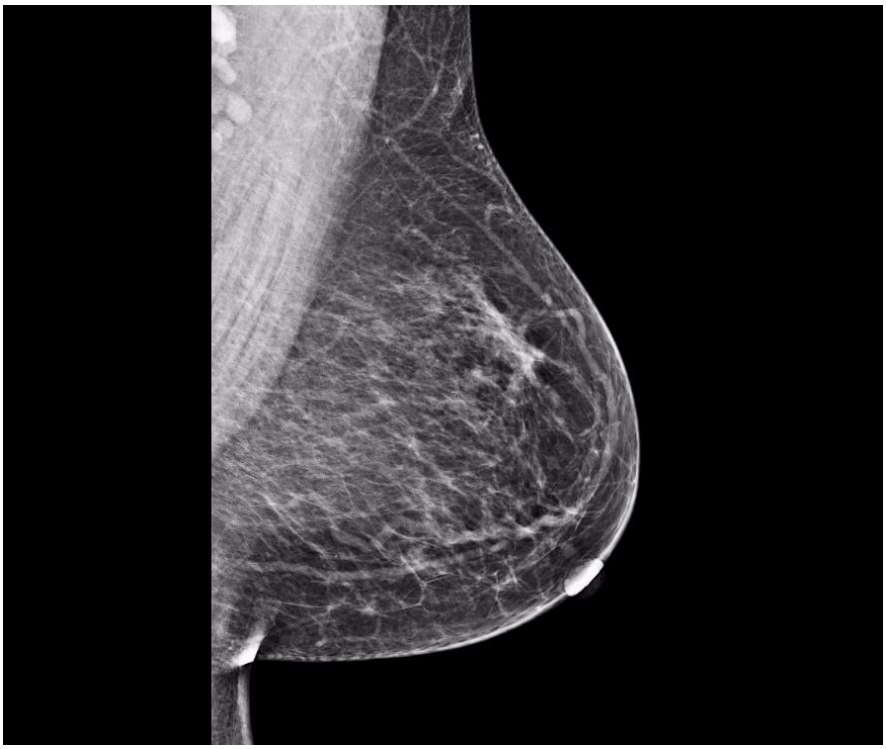

Source: https://undergradimaging.pressbooks.com/chapter/introduction-to-breast-imaging/

Screen-film mammography was long considered a "gold standard" for screening breast cancer. As well as being able to provide adequate visualization of abnormalities in soft tissue, its specific resilience is the ability to portray subtle calcifications. Screen-film mammography's most essential

and widely recognized shortcomings are correlated with its restricted dynamic range, contrast characteristics, proneness to inadequate conditions for film processing, and granularity. It also introduces severe limitations, despite the presence of dense glandular tissue, in detecting very subtle lesions. Those limitations were well addressed during digital mammography's preliminary development phases. Due to the advent of digital mammography, which provides wide dynamic range and provides the simplicity of digital image manipulation, communication and archival, additional investment to develop improved screen-film technology is unlikely [11].

The term "digital mammography" is used for any technology that uses a single or multiple sensor unit to capture an electronic image of the x-rays transmitted through the breast that may be electronically viewed, processed, and transmitted. Currently, nearly 36 percent of all mammography units in the U.S. are digital, and with the higher data throughput, it is possible that more than 59 percent of the exams will be carried out using digital mammography [12]. Clinical studies evaluating digital mammography with screen-film mammography in a screening population indicate equivalence for cancer detection, and digital mammography performed significantly better with dense breasts for pre- and postmenopausal women younger than 50 years.

Ultrasound is an imaging modality that utilizes sound waves in order to produce body images for examination purposes. [13] The use of ultrasound in breast, liver, prostate, ovarian, pancreatic, thyroid, uterine and kidney tumor detection is perceived to be a popular method of diagnostic imaging. During the ultrasonic test, high-frequency sound waves pass through the breast and are transformed into images presented on a digital display. The best way to determine whether the abnormality is solid (for example, a benign fibroadenoma or cancer) or fluid-filled (such as a benign cyst) is to perform an ultrasonic examination when detecting an abnormality on mammography, or when detected by physical examination. Ultrasound can determine the internal structure, morphology orientation and outlines of lesions from multiple planes with high resolution in both thick, glandular structures and primarily fatty breasts. [14] Between those attributes, important factors to consider when classifying a lesion are the surrounding tissue, size, margin contour, lesion border and dorsal acoustic attributes. Ultrasound is unable to assess whether a solid lump is malignant. The major utilization of ultrasound is to direct the biopsies.

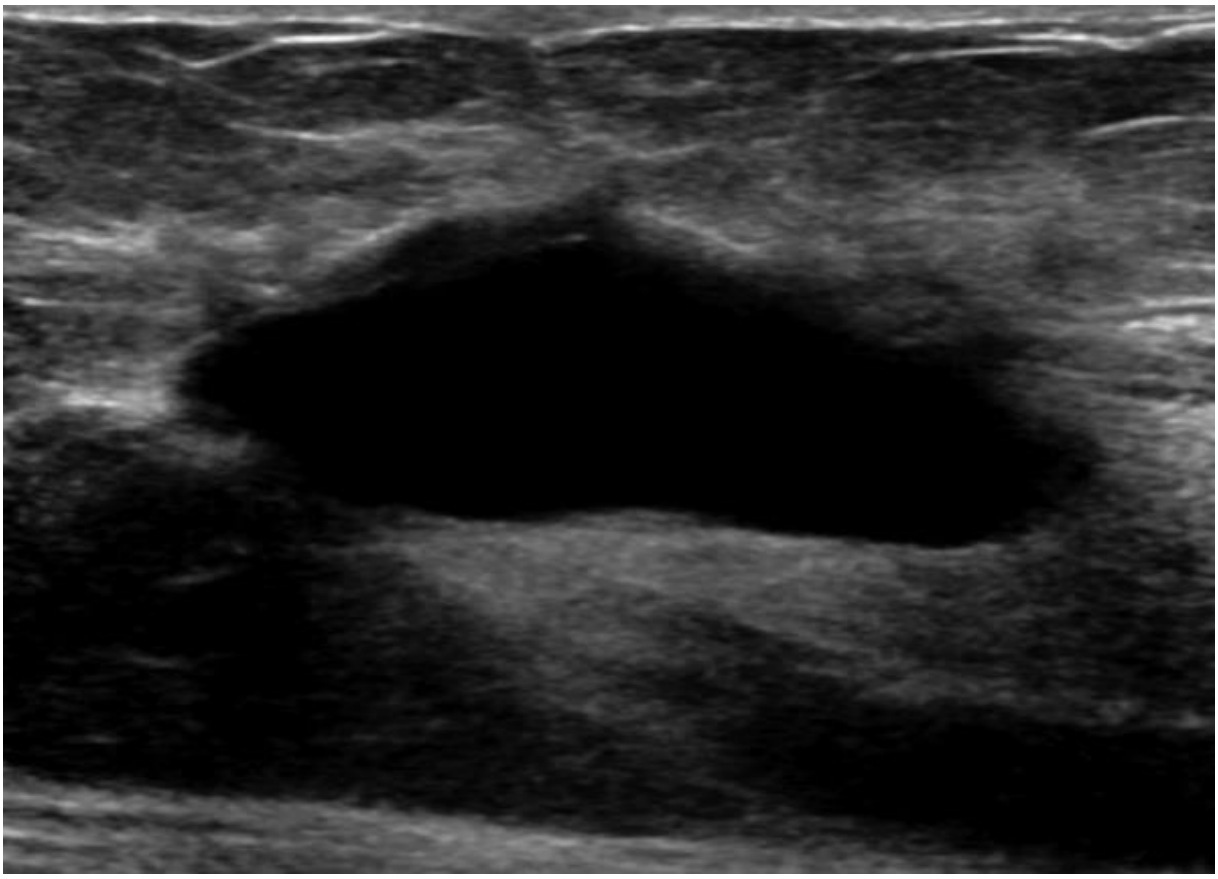

Figure 6: A normal breast ultrasound image.

Source: https://iame.com/online/screening_breast_ultrasound

Another imaging technique is Magnetic Resonance Imaging (MRI) used for breast cancer. The last two decades, there has been an increased number of MRI referrals. The primary advantage of MRI efficiency is based on the superior ability to detect ipsilateral and contralateral diseases opposed to mammography and ultrasound. Schelfout et al found in a prospective trial that MRI identified 96 percent of multifocal / multicentric disease, whereas mammography and ultrasound showed only 28.6 percent and 26.5 percent respectively [15]. Considering the histological forms of breast cancer, it is well documented that invasive lobular carcinoma has a greater frequency of multifocal, multicentric, and contralateral pathology opposed to invasive ductal carcinoma.

MRI is achieved by using a high-amplitude magnetic field and radio waves. The MR magnetic field aligns all the protons in the body in the direction of this external main magnetic field. Broadcasting a radio wave through the examining body area to perturb the protons and when it stops, the protons align back with the magnetic field. [16], [17] Once they move back into alignment with the magnetic field, the protons release energy. Receiver coils covering specific regions of the patient's anatomy i.e. knee coils, head coils, etc. detect this liberated energy and is

then transformed into electric signal. Through a series of sophisticated, computer-based mathematical calculations the original location of the generated signal is detected and positioned into an image matrix for display and analysis. Different tissues are described as higher or lower signals in MRI examination. The signal represents the energy emitted by the perturbed protons as they come back into alignment with the magnetic field. The contrast of the examined tissue changes on the basis of the image protocol parameters set by an MR Technologist under the supervision of a physicist ensuring optimal image quality. As a result, the acquisition of this set of images is called an MRI series, depending on the parameters set. [17] Two basic contrasts are achieved from the acquisition process, which in one body fluids appears with low signal density (T1 contrast) while the other high signal intensity (T2 contrast). This differentiation in the appearance of tissue can be utilized to evaluate whether pathology is present.

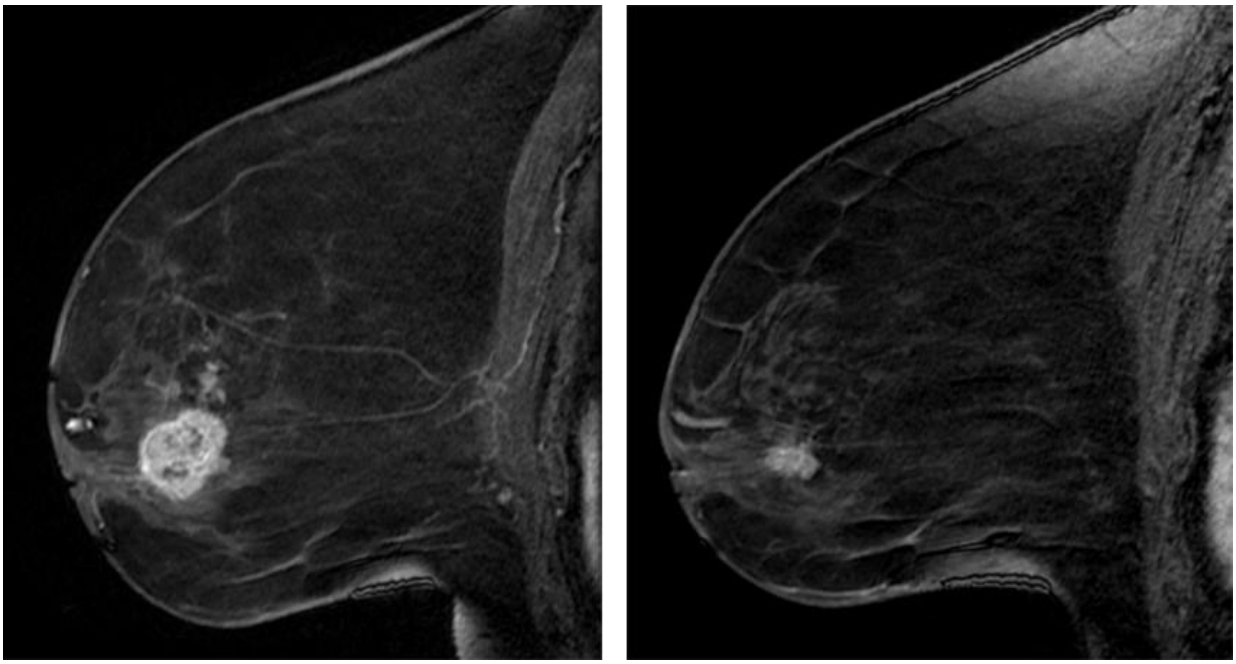

Figure 7: A display of a fat suppressed T1 MRI (left image) and a fat suppressed T2 MRI (right image) of a breast. Source: [18]

A body coil that generates the radio waves and a dedicate surface receiver collects the radio waves are utilized to produce the images is surrounding the body section of interest for MR. Different coils exist for various anatomical regions i.e. knee, head, breast, etc. While it remains a safe imaging modality, patients with known hyper-sensitivity to contrasting agents should not have contrast MRI. This is because of some of the MRI examinations require the injection of Gadolinium-based contrast agents. This imaging modality uses magnetic field of very high intensity to produce images. There are possible dangers associated with accidents involving the

form of missile, where ferromagnetic artifacts are easily drawn into the MR magnet. Furthermore, implanted objects can interfere with the magnetic field in patients such as cochlear implants, pacemakers and leads, aneurysm recordings, and other medical devices. In order to avert serious adverse events related to magnetic field accidents, patients need thorough monitoring by the clinicians and the medical physicists.

MRI demonstrates incredible anatomical description and offers the best anatomical representation of any of the imaging techniques. [16] Additionally, MR image sequences which are able to identify differential metabolic activity, i.e. MR spectroscopy, throughout the tissue can be extended to the evaluation of brain activity, i.e. functional MR (fMRI). [19] Furthermore, MRI may be also utilized to describe the flow of blood in the vascular system, i.e. MR perfusion based on dynamically acquiring a series of T1 weighted images before, during and after the injection of the gadolinium-based contrast agent. Therefore, MRI is one of medical imaging most crucial and flexible imaging techniques.

1.4. DCE MRI for breast cancer

Tumors growth beyond a few millimeters in size is achieved by the forming of new blood vessels which deliver metabolites and oxygen. [20] A variety of factors cause this angiogenesis, that are mainly due to tissue hypoxia in the core of the tumor and largely due to tumor host associations that generate a range of agents, most significant ones being the endothelial growth factor (VEGF). [21] The vessels created are different from ordinary tissue vessels because they are heterogeneous with many warped and twisted capillaries with fragile walls. There are several high-vascular density arteriovenous shunts and regions which are interspersed with hypoxic areas. VEGF is a glycoprotein which acts on the receptors of tyrosine kinase. [22] Widened endothelial fenestrae and an immature basement membrane lead to defective capillary walls.

Binding VEGF with endothelial cell receptors leads to higher capillary porosity, permitting the leak of plasma proteins and endothelial cells into the extracellular environment. The expression of VEGF has a positive correlation with the Microvessel Density (MVD). [23] Due to the relative increase in vascularity present in many malignancies, such as breast, primary rectal and colorectal cancer, in relation to normal tissues, intravenous contrast has been used to great effect in MRI, allowing for better con-spicuity of tumors. There are various types of the contrast agent used in magnetic resonance (MR). They can be categorized as per their characteristics including their metal center form, magnetic properties, chemical structure and bio distribution. Those utilized in contrast-enhanced dynamic (DCE)-MRI trials are usually extravascular and extracellular. [22] While mostly injected intravenously due to their liquid form, these contrast agents can also be administered orally.

The contrast agents (CA) most commonly utilized in cancer screening are gadolinium (Gd) based. Cas have a low molecular weight that allows easy passage into the extravascular area, especially in which the vessels are porous and they are intravenously injected. [24] Such contrast agents do not traverse the membranes of cells and stay in extracellular space. The capacity to monitor contrast enhancement over time has contributed to information being accessible concerning the condition of tissue microvasculature. DCE-MRI demands systematic imaging prior, during and afterwards an injection of a contrast agent across the entire anatomical area. The accuracy of the DCE MRI has been improved by simple workstation measurements of enhancement proportions and signal shift plotting over time, permitting the distinction of benign and malignant breast cancer. [25] It has been established that research of sophisticated pharmacokinetic modeling may lead to additional useful tumor-related information that can possibly be utilized as a biomarker for patients with phenotypes or as a monitoring tool for treatment-response. [26]

The effects of the contrast agent on hydrogen protons in tissue water are expressed in the alterations in the signal strength of a contrast-enhanced MRI study. Choosing the image sequence is required to optimize the effects of T1 or T2 relaxation. T1-weighted examinations are frequently conducted with short repetition time (TR) and echo time whereas T2-weighted imaging is mostly produced utilizing echo planar imaging with long TR and echo time. Fat suppression may be enforced with

the goal to improve area visibility. The technique of image acquisition implied in the dynamic imagery of a lesion depends on the information needed. [27]

Dynamic contrast-enhanced MRI (DCE MRI) has been utilized as a tool to increase diagnostic accuracy and to enhance non-invasive characterization of lesions. This became widely used in the field of breast imaging. Commercial workstations have a range of basic analytical tools for describing signal curves over time, maximal slope, time to peak (TTP) and maximum enhancement. The TTP is the time required after contrast injection for the signal to reach its maximum value. TTP has been proved effectively in the identification of malignant lesions. It became apparent that tumors are quite heterogeneous with several displaying a gradual increase in signal throughout time with a relatively homogenous enhancement pattern while others can display a malignancy-specific rim enhancement with a drastic increase in signal with an early peak and a malignancy-typical washout pattern. [28][29]

There is no gold standard for measuring the physiology of tumors and for verifying the pharmacokinetic measurements obtained with this method. Many experiments associated pharmacokinetic parameters with clinical outcome or used histopathology with tumor grade, tumor size, expression of MVD, lymph node status, or expression of VEGF in quantifiable prognostic factors. The slope of the enhancement curve is correlated with MVD and it has been observed that enhancement characteristics are closely related with the nodal status of a breast tumor and the histological grade. Objective measurements of tumor response such as adjustments in tumor size or volume are used as the end point in response-monitoring studies. [30]

The effects of neo-adjuvant chemotherapy are monitored with response biomarkers. MRI has been extensively studied in breast cancer and has been demonstrated to be comparable to standard mammography and ultrasound imaging methods in assessing adjustments in tumor size. The use of MRI for evaluating neo-adjuvant chemotherapy in women with locally advanced breast cancer is documented in a substantial volume of research. [31] Most studies, though, are narrow, with subjective approaches and incoherent endpoints rendering it challenging to determine the value or reproducibility of this and the benefit of patient care to the clinician. In terms of planning surgery, it is accepted that MRI is inferior to mammography, ultrasound and clinical review to determining the severity of cancer after completion of chemotherapy.

Breast cancer studies were conducted to determine if any of baseline MRI variables could be utilized in order to estimate treatment response, but none discovered them beneficial to date. A precise evaluation of deficiency of responsiveness will enable the oncologist to turn earlier in-patient treatment towards a more efficient chemotherapy regime.

Evaluation of response to chemotherapy is done by using both Ktrans and ve. As a promising biomarker, Ktrans has been extensively used in many studies, where reduction more than 50% to be correlated to positive response to treatment (biopsy evaluation for confirmation). [32]–[34] It has also been demonstrated that the peak amplitude ve is efficient with a decrease in peak corresponding in response. [32] Nevertheless, the combination of volume changes with changes in enhancement ratio improves the monitoring sensitivity of patients who will obtain a maximum pathological response [35], [36].

Correlative research proved the ability of DCE-MRI as an imaging biomarker in forms of principle evidence. Nonetheless, large-scale randomized controlled research is needed to verify site-wide reproducibility and check established protocols for data acquisition and marker quantification [37].

1.5. Breast cancer therapy

Breast cancer treatments options depend on its stage and if it is metastatic or not. Considering that, breast cancer is treated with surgery, radiation therapy (RT), endocrine / hormone therapy (HT), targeted therapy and chemotherapy (CT).

The goal for nonmetastatic breast cancer is to eradicate the tumor from the breast and local lymph nodes while also preventing metastatic reappearance. Localized therapy is usually consisted of surgical resection and sampling or by removing the axillary lymph nodes preceded by radiotherapy to completely remove any left cancer cells. Subtype therapies include endocrine therapy, usually combined with chemotherapy, antibody therapy and chemotherapy on its own for severe stages of breast cancer. Regarding metastatic breast cancer, the goals are to prolong survivability and suppressing symptoms. Metastatic breast cancer remains incurable in almost all patients. The same treatments are used, while surgery and chemotherapy mostly for the suppression of the symptoms. [38]

Breast conservation operation is the standard strategy in the treatment of localized breast cancer, with neoadjuvant therapy preceding the operation to reduce tumor size. In general, surgery is accompanied by adjuvant therapy to ensure full rehabilitation and reduce metastasis risk. Furthermore, cancer cells which may not be seen during surgery may be eliminated by radiation to decrease the risk of cancer recurrence at the local level. Radiation therapy is the procedure of exposing cancer cells directly into high radiation levels. Combining chemotherapy and radiation therapy after surgery, there is a great possibility of a high shrinking of the tumor. Adjuvant therapy should be decided whether there is a certain predicted sensitivity to specific treatment methods while benefiting from their use or when there is a risk of relapse. [39]

Endocrine therapy is used for countering estrogen-promoted tumor growth. A standard endocrine therapy is consisted of oral antiestrogen medication daily, usually for 5 years depending on the menopausal status. Tamoxifen is a potent modulator of estrogen receptors that competitively prevents the binding of estrogen. [31]

Radiation therapy is a crucial procedure preceding surgery in order to remove any left cancer cells. Breast cancer radiation therapy may be given to the whole or portion of the breast (after lumpectomy), chest wall (after mastectomy), and regional lymph nodes. Post lumpectomy whole-breast radiation is a normal part of the therapy for breast survival. A meta-analysis of 10 801 patients found that radiation administration following lumpectomy was correlated with decrease of approximately half in breast cancer recurrence and one-sixth at 10 and 15 years in breast cancer deaths respectively. [40] Regarding adjuvant systemic therapies, the radiation's representative payoff was fairly stable in spite of the relative risk of breast cancer. Therefore, for patients with higher-risk cancer the actual benefits were greater, and alternatively, for patients with the lowest-risk node-negative tumors, the mortality benefit confidence interval was zero.

Prospective studies have investigated the effectiveness after lumpectomy of a shorter radiation course and how to classify patients who may recover from increased dose. [41] Whilst the historical typical dosage and post lumpectomy radiation schedule was 50 Gy over 25 fractions, more recent research has implicated that a hypo fractionated plan (approximately 42.5 Gy over 16 fractions) is as efficient for reducing the risk of local recurrence and, if not more efficient for cosmesis. [42] Consequently, according to current guidelines a hypo fractionated plan for whole-breast radiation is now "favored." In contrast to the whole breast, post-lumpectomy radiation to the partial breast is an approach that has been studied predominantly in lower-risk patients aged 50 years and older. While studies indicated that partial breast radiation was linked to a slightly increased risk of local recurrence and a slightly worse cosmesis, recent findings refute this, and consensus recommendations endorse non-intraoperative partial breast radiation in patients with low risk. Prescribing a radiation boost precise to the tumor bed enhances local control but not morbidity, and therefore should be perceived in patients at higher risk. Furthermore, prospective randomized studies have also shown that females 65 years of age and older or 70 years of age and older with low-risk breast cancer, entire breast radiation post-lumpectomy has no noticeable effect on distant relapse or morbidity (whereas omitting radiation contributes to low-risk loco regional event risk). [43]

Radiation from post mastectomy is radiation to the chest wall, often with a reinforcement to the mastectomy area and/or regional nodal radiation. A meta-analysis (N=8135) of randomized mastectomy radiation tests indicated that post-mastectomy radiation was not correlated with relapse or survivability outcomes in patients with negative lymph nodes. Nevertheless, application of post-mastectomy radiation in patients with healthy lymph nodes has been affiliated with increased locoregional and relative relapse possibility and mortality from breast cancer [31], [44]. Including regional nodal radiation (exposing the axillary, par clavicular, and/or internal mammary nodes) following either lumpectomy or mastectomy was correlated with greatly enhanced disease-free mortality, was not linked with overall mortality, and was associated with increased radiation toxicity such as pneumonitis and lymphedema. Nodal radiation is not universally administered even in node-positive patients due to the lack of overall survival benefit, but should also be regarded for patients with increased nodal disease burden or high-risk biology. [45]

Over the past decades, surgical treatment for breast cancer has developed considerably, with improvements directed at reducing the long-term cosmetic and functional complications of local therapy. [46] The conventional techniques are either a total mastectomy, or an excision plus radiation based on extensive studies, presuming straightforward margins can be attained. These 2 methods have consistently been shown to be comparable in terms of relapse-free and overall survivability. Conservative surgery contraindications involve (1) the appearance of dispersed abnormal microcalcifications on breast imaging; (2) specific collagen-vascular diseases, e.g. scleroderma; (3) disease which cannot be handled by surgical removal of a single region of breast tissue with a reasonable cosmetic result, except in highly selected patients; (4) healthy pathological margins following lumpectomy; and (5) leading up breast radiation therapy. The axillary lymph nodes should be treated separately from breast surgical therapy. Lymph node removal provides both a therapeutic significance (removal of cancer cells) and a diagnostic function (defining breast

cancer's anatomical degree). [47] Surgical judgment-making is focused on whether activity of the axillary lymph node is visible at diagnosis and whether systemic neoadjuvant therapy is being delivered. Axillary lymph node dissection (ALND), which maintains the standard treatment for patients with clinically apparent axillary involvement in the diagnosis who undergo surgery as initial therapy, was the standard path to axilla before clinical studies found that there is no substantial difference in local relapse or survival results in women with clinically node-negative (cN0) breast cancer among women who had complete ALND and women who had sentinel lymph node (SLN) biopsy, with conversion to ALND only if the SLN was positive. [48] The surgical treatment is emerging for patients receiving systemic neo-adjuvant therapy. Several observational randomized studies and a recent meta-analysis indicate that neo-adjuvant chemotherapy has expanded the availability of patients for breast-conserving therapy without sacrificing long-term results. A field of active investigation is the effective management of lymph node disease following neoadjuvant therapy.

Chemotherapy remains an effective procedure in many patients with stage I-III breast cancer, given the related short- and long-term risks. Considered the only systematic treatment with established efficiency in triple-negative breast cancer, and a major alternative to endocrine therapy or controlled therapy in breast cancer patients. [49]

A study utilized a cohort 100 000 women engaged in controlled early breast cancer chemotherapy tests found that a high-dose anthracycline containing chemotherapy regimen (opposed to no chemotherapy) greatly reduced 10-year breast cancer survival rate at about one-third, with most survival benefits emerging during the first five years of treatment. [50]

Similarly to adjuvant endocrine therapy for hormone receptor tumors, chemotherapy correlates with higher-risk tumors providing an increased total benefit. Several specific regimens of neoadjuvant and adjuvant chemotherapy may be recommended for early breast cancer. Generally, the regimens of different chemo therapies are all sensible options for smaller-risk patients considering the benefits of chemotherapy are lower and toxicity is carefully managed. All anthracycline and taxane-containing chemotherapy regimens demonstrate the highest reduction in risk and remain the ideal option for high-risk patients. Generally, the use of anthracycline in patients with more involvement of the lymph node and with triple negative disease tends to be the most significant. For patients receiving a full cycle of neoadjuvant chemotherapy containing anthracycline and taxane, if residual disease is detected during surgery, further treatment remains uncertain. [31]

In particular, chemotherapy is given to all women with breast tumors greater than 5 mm, although with negative axillary nodes. The only drugs approved by the Food and Drug Administration (FDA) for treating non-metastatic disease are chemotherapeutic agents. Since defective repair of DNA damage is a biological characteristic of some tumors, triple-negative disease has been of interest to investigate the DNA cross-linking platinum chemotherapies. Two studies have recruited breast cancer patients to undergo neo-adjuvant chemotherapy both with and without carboplatin, and both have reported substantial improvements in pathologic complete response (pCR) with the

inclusion of carboplatin in the operation. Although, in the carboplatin - containing group, only one of the trials showed significant improvement in disease-free survival, and in this scenario, the other elements of the chemotherapy regimen were not coherent with conventional therapy and did not include an alkylating agent [31]. Hence, the importance of platinum salts in treating patients with triple-negative breast cancer in stage I-III remains unclear.

Another treatment of cancer is Neoadjuvant therapy (NT). NT is the administration of therapeutic agents prior to the main treatment in order to reduce the extent or size of the cancer. That will result in an easier operation of surgical removal of the tumor and reduce any additional residues that might have existed. NT can either be chemotherapy, radiation therapy or hormone therapy and is usually utilized early on patients with not advanced cancer to prevent any expanding of the tumor.

In our case, neo adjuvant chemotherapy (NAC) was administrated to the patients in order to shrink tumors volume for a better surgical operation. [51] NAC was introduced in 1980s on patients with locally advanced tumor in order to transform the inoperable tumors into operable ones. [52] After the positive results of NAC, with its major benefit being the increase of breast conservation, researchers were urged to conduct an analysis on randomized trials to evaluate NAC effects on earlier stages. [53]

In a recent review comparing adjuvant and neo adjuvant chemotherapy studies it was perceived that the outcome is equivalent with the difference that NAC can help in the preservation of the breast. Additionally, NAC can help decrease any adverse events while also having no negative affect in the loco regional control of the tumor. Another benefit of NAC is the recovery of patients before surgery. Patients without NAC have stressed their immune system after surgery and the chemotherapy followed can be harmful. However, NAC patients have shown that their recovery time from chemotherapy was faster and enough to move into surgery. [54] Furthermore, NAC facilitates the monitoring of tumor response which can save time or unnecessary exposure to harmful side-effects that might occur to a patient. [55]–[57] For these reasons, NAC is an excellent therapy to determine the most efficient therapy plan for each individual. Thus, enabling us to explore further its capabilities and effects by trying to predict each Breast cancer patient therapy response and help personalized medicine move further.

1.6. State of the art in predicting NAC

Predicting NAC outcome of breast cancer patients can help clinicians move towards personalized medicine and individual-specific planning of treatment. For this reason, researchers have shown a lot of interest in predicting NAC as early as possible, even at baseline before therapy administration.

Researchers explore the predictive power of imaging biomarkers by using quantitative and semi-quantitative analytical methods in DCE-MRI. Ah-See et al. [58] discovered that ktrans had great predictive ability in a cohort of 28 breast cancer patients, achieving an AUROC score of 93%, sensitivity at 94% and specificity 82%. Additionally, important predictive value proved to have the Apparent Diffusion Coefficient (ADC) which was acquired from the Diffusion Weighted Imaging (DWI) data, revealing inclination of responding to NAC in patients with low ADC on baseline exam[59].

All the above studies, however, use functional information in the form of pathophysiology, image-derived markers to predict the outcome of NAC therapy. Due to these approaches, spatial structure of the image intensities is often overlooked, however, they can reveal useful information concerning tumor heterogeneity. Since it is well-known that tumor heterogeneity has a great predictive ability [60] it makes sense to investigate it along with texture radiomic features which conceivably will lead to improved predictability in the NAC outcome particularly if we consider changes in texture patterns over the examination time.

Texture analysis was used to predict the outcome of NAC treatment for breast cancer. In [61], It is shown that the textural features derived from breast cancer DCE images were found to be more reliable two minutes after contrast agent (CA) injection to predict patient response to therapy using a cohort of 89 patients, 40 of whom were responders and 49 were non-responders. The features that were derived 2 minutes after the CA injection showed a better predictive power that the features that were derived from all time points of the exam.

In a research of Agner et al. [62], texture kinetics were introduced as novel technique to categorize breast tumor into benign or malignant classes. While the design requirements were a difficult task, the textural kinetic characteristics and morphological parameters in the classification process were very accurate. Using a cohort of 41 patients (17 benign and 24 malignant), a probabilistic boosting tree (PBT) classifier resulted in 90% accuracy, 95% sensitivity, 82% specificity and AUROC 92%.

Another research from Thibault et al. [63] was conducted applying texture analysis in quantitative and semi-quantitative DCE-MRI data of 38 patients. After the first cycle of NAC therapy using 1043 texture features extracted from 13 parametric maps, they achieved a perfect discrimination of responders and non-responders (100% sensitivity and specificity).

Michoux et al. [64] utilized a cohort of 69 patients with invasive ductal carcinoma of the breast for analyzing and extracting morphological and biological parameters. Kinetic and BI-RADS features

have been extracted for each lesion texture, while ROC analysis and leave-one-out cross-validation assessment measure their performance. Their results shown that four pre-NAC parameters were able to predict the responders to NAC with sensitivity of 84%.

In [65] Teruel et al. explored the role of DCE MRI texture analysis in a cohort of 58 patients with locally advanced breast cancer, for the prediction to NAC therapy. Utilizing gray level co-occurrence matrix, sixteen features were derived from every post contrast acquisition. A number of statistically significant texture characteristics were found to be adequate predictors 1 to 3 minutes after injection of CA.

Furthermore, as aforementioned, this thesis contributed to 2 researches. While both explore the prediction of NAC outcome, the first, as mentioned, investigates the strength of textural kinetics, while the second, explores the predictability power of multi-scale Gabor filtered texture features.

Multi-scale classification common and main problem is that the feature space is highly dimensional since it contains features extracted from different scales. In [66] multi-scale texture images were created using scaled by-products up to second order and then using combined classifiers rather combining features in order to overcome the problem of high dimensionality. The features extracted at each scale were used in different classifiers and the results were merged using a fixed merging rule for selecting texture classes. Many examples of multiresolution techniques have been used for texture analysis in literature including: multiresolution histograms [67], multi-scale local binary patterns [68], multiresolution Markov random fields [69], wavelets [70], [71], Gabor filters [70], [72] and Gabor wavelet filters [73].

In [74], DCE-MRI was utilized to assess the response to NAC treatment of the breast cancer patients. Using a cohort of 54 patients which underwent two chemotherapy circles, a multivariate analysis with cross-validation was performed on features which characterized the kinetics and the morphology of the contrast agent in both early and late phases of the exam. Also, utilizing a Receiver Operating Characteristic (ROC) analysis, the results for predicting the treatment outcome were 73%.

In another study by Johansen et al. [75], DCE – MRI exams were used as a predictive tool to early chemotherapy response and the evaluation of 5-year survival in patients. Relative signal intensity (RSI) as well as area under the curve (AUC) were both calculated from the DCE – MRI examinations for the comparison with the clinical treatment response. Additionally, a Kohonen and probabilistic neural network analysis was conducted for the prediction of 5-year survival. The results for the prediction of clinical treatment response were above 90% while the neural network analysis in the range of 80% to 92% in the prediction of 5-year survival.

Additionally, in [76] an evaluation of the response to chemotherapy of breast cancer patients using radiomics features of the DCE-MRI was conducted. More specifically, 57 patients exams were analyzed, which 47 were responders while the 10 were not, according to the RECIST criteria. One hundred and fifty eight radiomic features were extracted from MRI examinations to characterize

the heterogeneity of the tumor and to discriminate the background of the image. Using a Wrapper Subset Evaluator classifier and an area under the curve calculation to evaluate the classifiers performance it was shown that the average accuracy for the prediction to chemotherapy was 70.3%.

In [77], a cohort of 586 breast cancer patients were used along with the multi parametric MRI examinations available for the prediction of NAC response. All of the imaging examinations were before the NAC of each patient. Extracting features from coarse to fine, a set of 4 radiomic features was created. Using an area under the curve analysis, the average accuracy from all the different parametric MRI examinations was 79%.

1.7. Scope and research questions

This thesis is focused on examining the importance of textural features in DCE-MRI towards the prediction of NAC. DCE-MRI is an efficient imaging tool for breast cancer used extensively all over the world. While RECIST and WHO criteria provide efficient evaluation of tumor response to NAC treatment, the heterogeneity of the tumor is often neglected due to the fact that such criteria focus on linear measurements such as the diameter of the tumor. For this reason, we proposed the use of reliable texture descriptors such as the Gabor filter, on the examination images in order to extract textural features that are then use for developing predictive models of NAC response (work done outside the scope of this thesis).

In this work, we use radiomics to extract temporal texture features, utilizing Dynamic Contrast-Enhanced (DCE) MRI 3D image volume, thus examining the change of texture in time. Exploring this change in tumors structure, we hypothesized that radiomic features can help improve the prediction procedure due to the use of both dimensional features and textural features. Radiomics analysis is really promising for revealing substantial tissue properties offering more precision in the management of cancer patients leading to a more personalized diagnosis.

However, texture can be extracted at different resolutions/scales. Texture contains significant information at different scales, thus making scale a continuous variable rather than a simple parameter. We propose a framework of Gabor filtering using a set number of orientations and scales. Gabor filter provides concurrent optimal resolution in both spatial and frequency domains, considered by many contemporary computer vision scientists to be comparable to the human vision system. Gabor filters have been used effectively in several implementations, including texture analysis and segmentation. The framework's pipeline includes a pre-processing filtering of the images using a Gabor filter bank of different scales and orientations following the extraction of radiomic features. Using this approach, we examined whether Gabor-based multi-scale and orientation filtering improves the predictive power of radiomic features and how stable they are in corresponding feature importance in the prediction algorithm.

More specifically:

- Extracting radiomics features in DCE MRI of breast cancer patients for the prediction of the tumor response

- Development of a multi-scale Gabor filter framework investigating the effect of scale of textural features in their predictive strength regarding NAC prediction

1.8. Outline

This thesis is outlined as follows:

- In the first chapter, Introduction, basic theoretical concepts, breast and breast cancer description as well as epidimology, state-of-the-art research and projects is provided as well as the rationale for conducting this thesis

- In the second chapter, an explanation of texture kinetics and how they are used in this work is provided.

- In the third chapter, Gabor filters are introduced focusing on how they can provide useful biomarkers using radiomic texture features.

- In the fourth chapter, the results of this thesis are presented and explained thoroughly as part of a machine learning prediction study.

- In the last and fifth chapter, Discussion, we discuss our results and methods and propose new ideas for extending this work and its applications.

- At the end are listed every source of literature information.

1.9. List of Publications

This thesis has contributed to two publications. The first publication was on a research trying to use texture features derived from the patients' exams original images and wavelet filtered images to predict the response of NAC treatment. The second publication was on a research to predict the NAC treatment using the texture features derived from a Gabor filtered image of the patients' exams. The contribution of the thesis was on the extraction of the texture-Radiomics features and the development of the Gabor scale-orientation framework.

1. Kontopodis, E., Manikis, G., Skepasianos, I., Tsagkarakis, K., Nikiforaki, K., Papadakis Z., G., Maris, Th.G., Papadaki, E., Karantanas, A., & Marias, K. (2018). DCE-MRI radiomics features for predicting breast cancer neoadjuvant therapy response. 10.1109/IST.2018.8577128

2. Manikis G., Venianaki M., Skepasianos I., Papadakis Z., G., Maris T., Agelaki S., Karantanas A., Marias K. (2019). Scale-Space DCE-MRI Radiomics Analysis Based on Gabor Filters for Predicting Breast Cancer Therapy Response. 994-1001. 10.1109/BIBE.2019.00185.

1.10. Dataset Description

The database used in this work is an open for public available data set from The Cancer Imaging Archive which comprises of a cohort of histologically-proven breast cancer stage II and III, 59 patients.[78] Included scans are: DCE, DWI MRI and PET/CT, before the starting NAC treatment, after the first cycle and before the end of it. Classification of the patients was also available and was derived according to the biopsy acquired at the end of the NAC treatment. Classification was defined as responders (pCR) and non-responders (non-pCR). According to Sataloff [79], response to NAC was determined as the inadequacy of tumor residual in breast and lymph nodes.

Out of the 59 patients, only 20 had PET/CT exams thus excluded from this work. Furthermore, 4 patients had only one DCE exam which lead us excluding them because we studied those who had two DCE exams. Resulting, patient cohort was reduced to 35 patients out of which, 12 were responders (pCR) and 23 non-responders (non-pCR). Additionally, any patients with third exam were included, however the third exam was not analyzed.

DCE scans were obtained using a bilateral breast coil with 16 channels on a 3.0 T Philips Achieva MR scanner. Regarding DCE protocol, 20° flip angle, TR 7.9 ms, TE 4.6 ms, 192x192x20 image resolution, 220x220 mm2 field of view (FOV), 5mm slice thickness and 25 dynamic acquisitions with 16 seconds temporal resolution was used. The gadopentetate dimeglumine (Gd-DTPA) CA was used with a power injector using 0.1mmol/kg. The detailed description of the therapeutic regimen and the acquisition protocol is provided in [80].

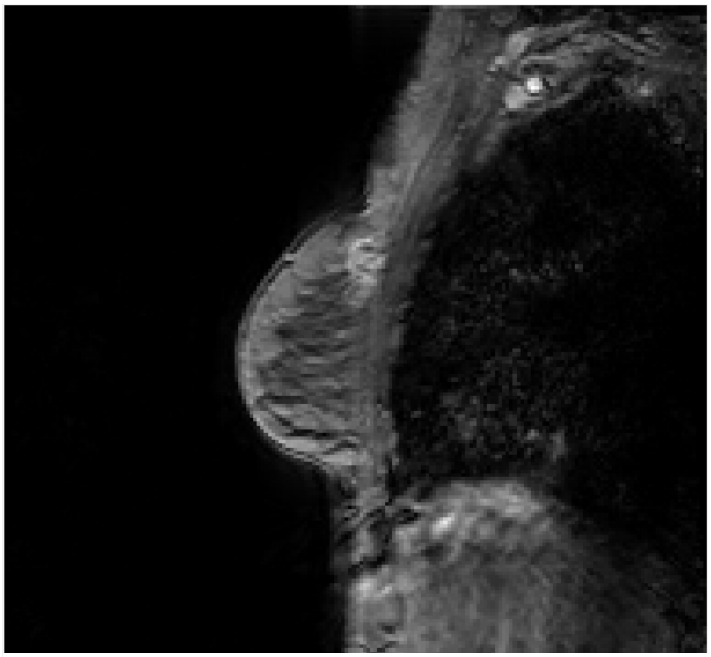

Figure 8:A preview of the images included in the dataset used.

2. Texture Kinetics

2.1. Introduction to texture

Image Texture in image processing is a method to quantify the characteristics of the patterns of an image which is perceived as texture. Image texture provides us data on the spatial arrangement of the signal strength in an image or area of interest in an image. While a specific definition of texture does not exist yet, commonly accepted are “Reference to properties that represent the surface or structure of an object”, “Repeated patterns of local variations in image intensity”.

According to Haralick “Despite the importance and ubiquity in image data, a formal approach or precise definition of texture does not exist”. [81]Image texture is an important property, since it can provide useful information, especially for classification of images. In order to understand and perceive texture, humans use meaningful features of the image. Most important are spectral, textural, and contextual features. Textural characteristics provide information on the temporal distribution of gray-tone variations within an image. Spectral features contain the average tonal variations while contextual features describe the groups of pixels around the area of interest. Texture and tonal properties of an image are closely related. Texture is the dominant property in the case of a small area with wide variation of discrete tonal features, while grey level is dominant when the variation is lower.

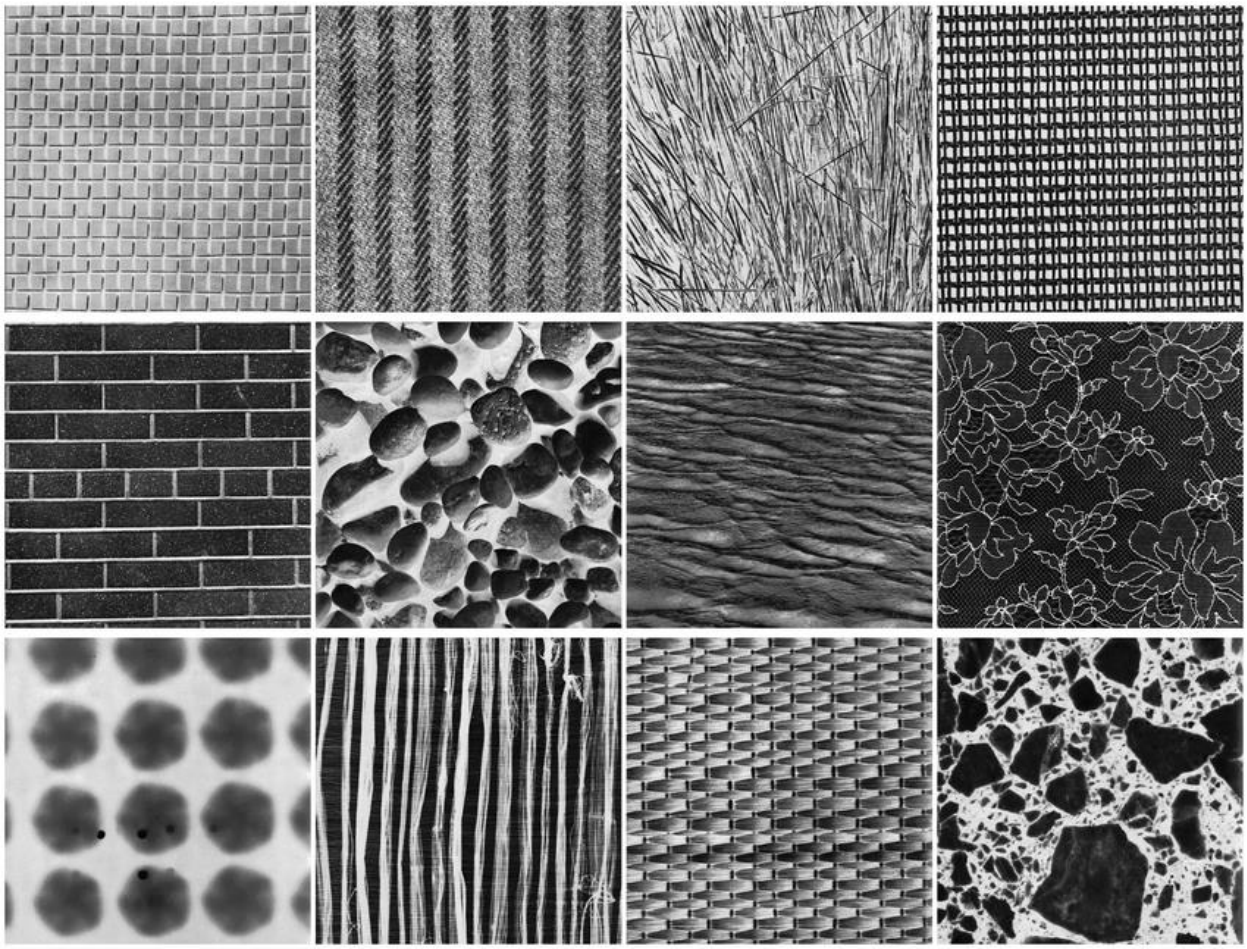

Figure 9: Brodatz texture images are used extensively as a gold standard for texture classification, segmentation and feature extraction [82].

Discrete tonal features can be expanded to the grey-level primitives. Which are distinct regions in an image, defined by both its grey-level and region properties. Spatial distribution and grey-level primitives are able to characterize texture. Texture can be described as micro texture if the spatial interaction is local and the grey level primitives are small in size. If the grey level primitives are larger in size and regularly organized in the image, then the texture can be described as macrotexture. For that reason, examination scale is very important in the textural description of the image. In other words, texture can change in appearance, depending at which scale it is examined. Increasing the scale, regions that had smooth texture, will now have fine and coarse textures. This should be considered before examining the texture of mammographic data, because the size of the region of interest in this study varies a lot.

Researchers have also characterized texture as natural or artificial [83]. Artificial textures are mostly consisted of symbols which are part of a neutral background image. Autoregressive models and Markov random fields can create artificial textures, depending on the parameters given. However, natural textures are images which, for example, show brick walls, grass, water etc.

As mentioned, texture is a fundamental attribute of images which contains information of the arrangements of an image and the relationships between them. Texture can be characterized as coarse, smoothed, rippled, irregular and more. For that reason, researchers are using its information for segmentation and discrimination purposes. In this work, however, texture analysis and extraction of features will be used as a pre-process for the prediction of NAC treatment patients.

Texture analysis can be achieved using two methods. The first method is called statistical, which includes optical transforms, digital transforms, textural edges, structural element, grey-tone co-occurrence, autocorrelation functions and autoregressive models. Statistical methods have been used extensively, especially for the examination of micro textures. On the other hand, structural methods follow an idea that views each texture as groups of pixels placed in regular spatial distributions. Both of these methods are analyzed to a great extent by Haralick [84].

Temporal texture feature change or texture kinetics were introduced by [62], in which study, it was attempted to classify breast tumors into benign and malignant classes. Although being a difficult classification, it was shown that texture kinetics and morphological parameters provided adequate accuracy results.

In this study, temporal texture features are extracted from certain time points of each patient's exam. Four different time points were selected in both baseline and follow up exams. The first image set is before the injection of the contrast agent (TP1). This set of images has been chosen because they depict the anatomy without contrast agent and can serve as a control image. The second set of images is the peak enhancement (TP2), where according to literature, in breast cancer exams, peak enhancements is about 120 seconds after the injection of contrast agent [26], which in our study occurs at the 8^{th} time point considering the 16 seconds temporal resolution. This set has been chosen due to the optimum enhancement of the contrast agent. Additionally, the last time point of the exam considered, is called the end phase (TP3), which is when the contrast agent dynamics are stable. Finally, the difference between the first two selected time points was chosen (TP4 = TP2 – TP1) in order to take account only the enhancement of the tumor.

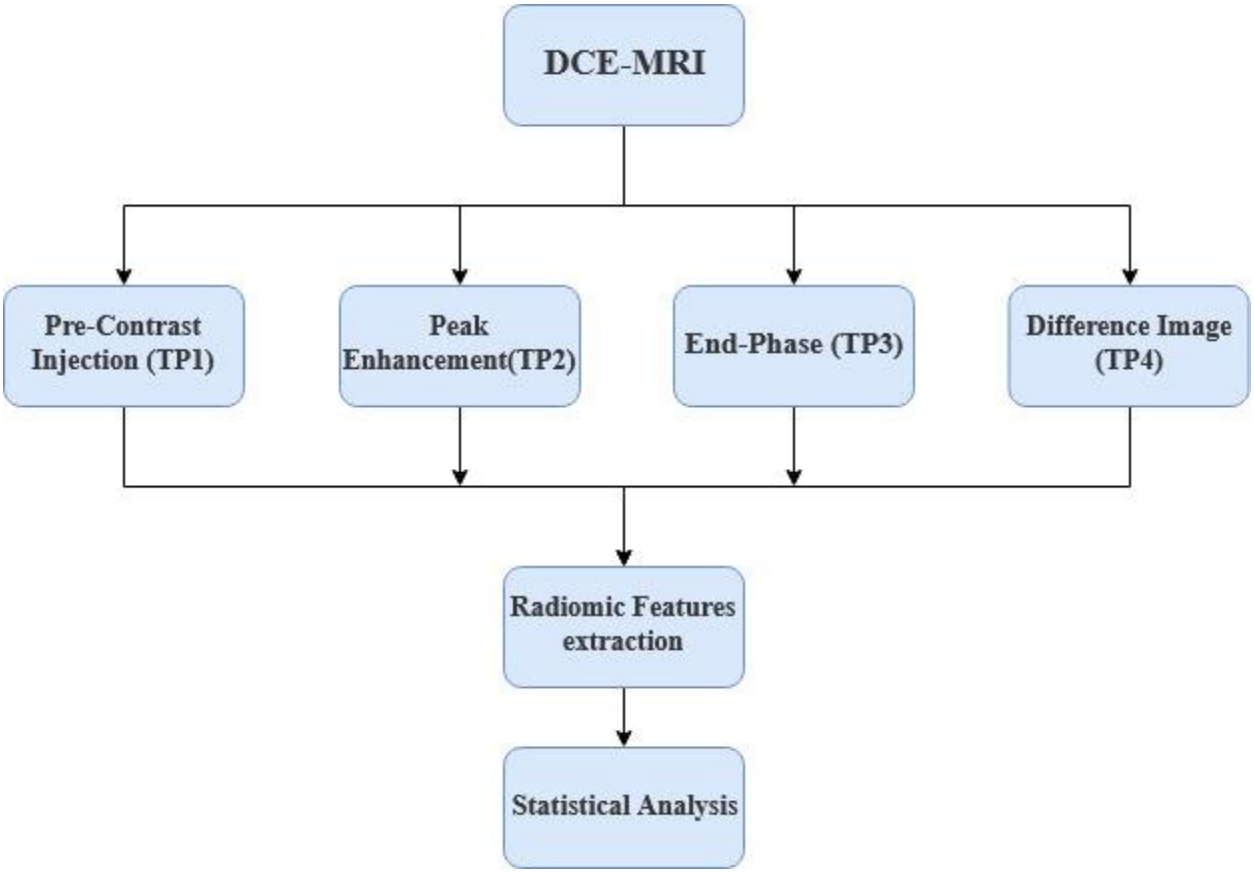

Figure 10: Pipeline of the proposed radiomic features extraction.[85]

In addition, Radiomic features derive a great number of quantitative features using statistics of the first and higher order applied to pre-annotated malignant areas of the 3D volume. In [85], we extracted from raw and filtered images a total of 1220 imaging features. First order statistics include histogram metrics, shape characteristics and second-order statistics relied on the Gray–Level Co-Occurrence Matrix (GLCM), Gray-Level Run Length Matrix (GLRLM) and Gray-Level Size Zone Matrix (GLSZM) were computed composing a large vector of 1220 features for each examined DCE-MRI exam. This computation was performed in Python using the PyRadiomics package [86]. More information is shown in the table below:

Table 1:All of the computed Radiomic Features used in our research

Radiomics		
First-Order	10 th percentile, 90 th percentile, Energy, Entropy, Interquartile Range, Kurtosis, Mean Absolute Deviation (MAD), Mean, Median, Range, Robust Mean Absolute Deviation (rMAD), Root Mean Squared (RMS), Skewness, Total Energy, Uniformity, Variance	
Second-Order	**GLCM**	Autocorrelation, Joint Average, Cluster Prominence, Cluster Shade, Cluster Tendency, Contrast, Correlation, Difference Average, Difference Entropy, Difference Variance, Inverse Difference (ID), Inverse Difference Moment (IDM), Inverse Difference Moment Normalized (IDMN), Inverse Difference Normalized (IDN), Informational Measure of Correlation (IMC) 1, Informational Measure of Correlation (IMC) 2, Inverse Variance, Joint Energy, Joint Entropy, Maximum Probability, Sum Average, Sum Entropy, Sum of Squares
	GLRLM	Short Run Emphasis (SRE), Long Run Emphasis (LRE), Gray Level Non-Uniformity (GLN), Gray Level Non- Uniformity Normalized (GLNN), Run Length Non- Uniformity (RLN), Run Length Non-Uniformity Normalized (RLNN), Run Percentage (RP), Gray Level Variance (GLV), Run Variance (RV), Run Entropy (RE), Low Gray Level Run Emphasis (LGLRE), High Gray Level Run Emphasis (HGLRE), Short Run Low Gray Level Emphasis (SRLGLE), Short Run High Gray Level Emphasis (SRHGLE), Long Run Low Gray Level Emphasis (LRLGLE), Long Run High Gray Level Emphasis (LRHGLE)
	GLSZM	Small Area Emphasis (SAE), Large Area Emphasis (LAE), Gray Level Non-Uniformity (GLN), Gray Level Non-Uniformity Normalized (GLNN), Size-Zone Non- Uniformity (SZN), Size-Zone Non-Uniformity Normalized (SZNN), Zone Percentage (ZP), Gray Level Variance (GLV), Zone Variance (ZV), Zone Entropy (ZE), Low Gray Level Zone Emphasis (LGLZE), High Gray Level Zone Emphasis (HGLZE), Small Area Low Gray Level Emphasis (SALGLE), Small Area High Gray Level Emphasis (SAHGLE), Large Area Low Gray Level Emphasis (LALGLE), Large Area High Gray Level Emphasis (LAHGLE)

2.2. Radiomic features extraction

As aforementioned, temporal texture features are extracted in order to predict the outcome of the NAC treatment. More specifically, we extracted spatiotemporal radiomic features from the selected time points. Radiomic features were introduced as the result of progressive computational approaches to medical imaging converting this data to quantitative descriptors of oncologic tissues. They are separated into five groups: size and shape-based features, descriptors of the image intensity histogram, descriptors of the relationships between image voxels and neighborhood area.

Texture analysis has been extensively used in medical data research since it can provide quantitative information of the disease. The major texture analysis approaches [87] are three: i) statistical, which are based on the spatial distribution of the pixels, ii) structural, which are based on the geometrical properties of the image, and iii) signal processing, which rely on filtering methods in the frequency or spatial domain. In this study we focus on signal processing techniques using Gabor Filtering, which is a multi-scale technique to quantitatively describe texture at different orientations and scales. The fundamental idea behind multi-scale texture techniques is that noteworthy information about the image structure is contained at different scales and not only at one. Thus, scale is not just a simple parameter but a continuous variable leading to the extraction of features at multiple scales, allowing for a multi-scale representation of texture.

Radiomic features are derived using certain algorithms, as shown in the table before, which analyze the patterns of certain areas depending on their intensity, connection and relationship. These algorithms will be explained below

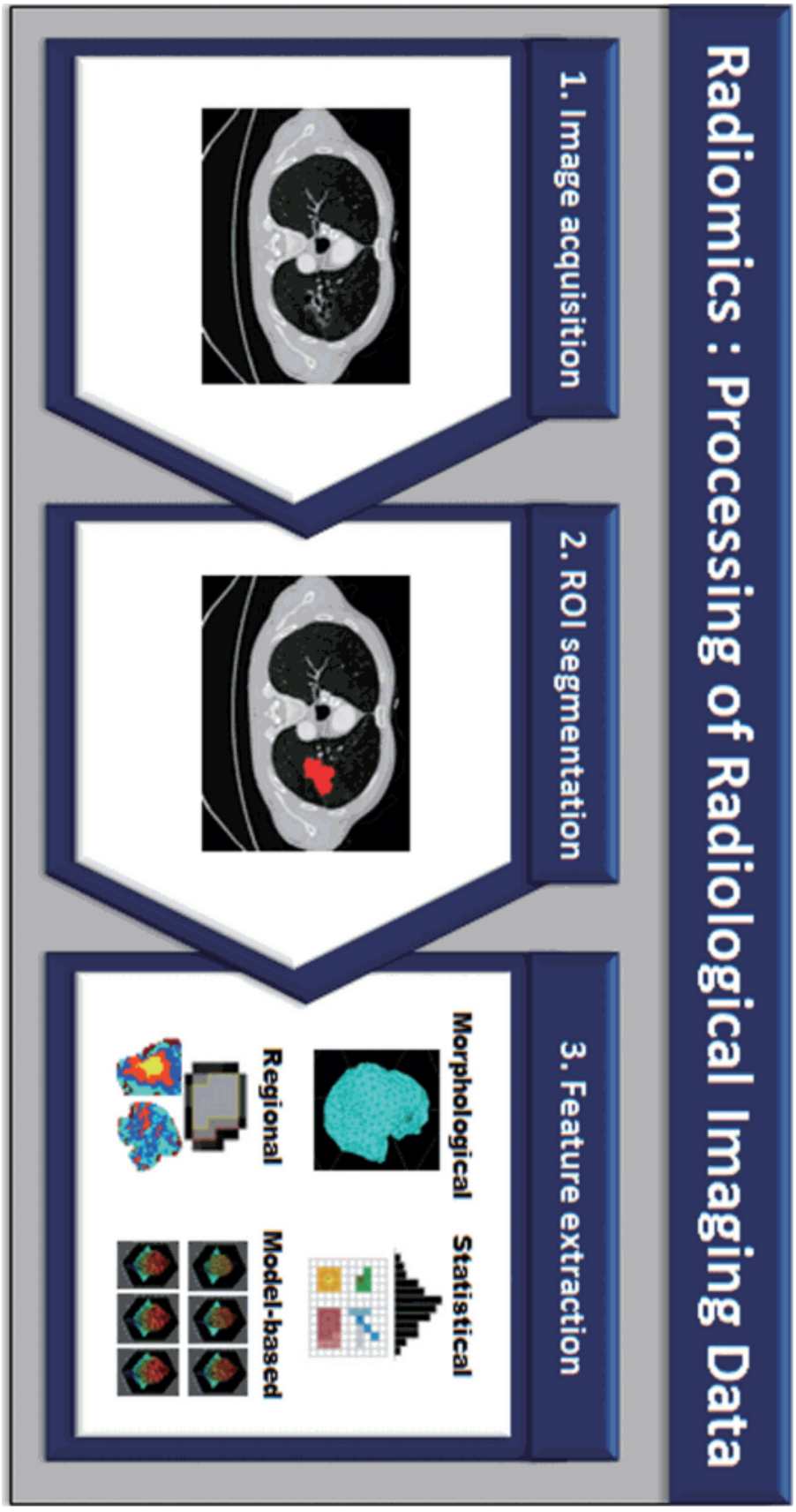

Figure 11: Procedure of radiomic features extraction [113]

2.2.1. Gray-Level Co-occurrence Matrix (GLCM)

Gray-Level Co-occurrence Matrix (GLCM) is a method of analyzing the intensity and relationship of the pixels in an image. Certain areas within an image can be characterized as texture, depending on their pixels' relationship, whilst helping us understand and extract more information about it (e.g. features). These features were first introduced by Haralick [81] and are used extensively as of today for quantifying image texture.

To calculate GLCM one must examine the image pixel by pixel. Starting with a single pixel, which is named reference pixel, the relationship between it and the pixels around it are considered. These pixels are called neighbor pixels and only a single one of them is examined in each application. This examination depends on the direction one is analyzing the image. This direction can either be right of it, left of it, above or below it. Additionally, a pixel offset is used for the analysis. In the illustration below, the pixel values in blue are the reference pixels while the green ones are the neighbor ones.

0	0	1	1
0	0	1	1
0	2	2	3
2	2	3	3

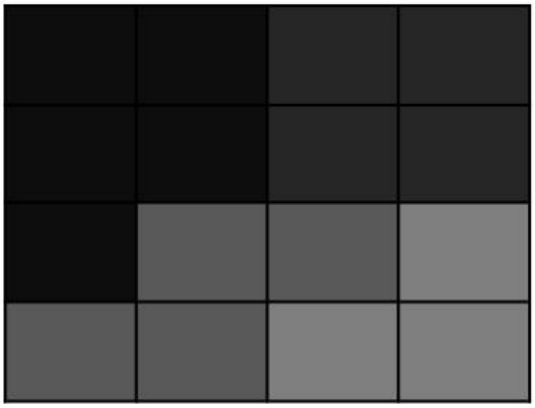

Figure 12: Example of a GLCM calculation using these images

Considering this illustration and using the east direction (right), counting the number of pixel pairs is how a GLCM is constructed. In this scenario, two cases of (0,1), (0,0), (1,1), (2,2) and (2,3) are counted with a single case of (0,2). Using this information, we can construct GLCM as shown below:

	0	1	2	3
0	2	2	1	0
1	0	2	0	0
2	0	0	2	2
3	0	0	0	1

Figure 13: Calculated GLCM outcome.

Additionally, constructing GLCM in one direction is not the only option. GLCM can be examined from several angles, for example four, which results into 4 different GLCM tables. Considering that, one can retrieve a thorough, circular investigation of the texture of the image. [88]

GLCM has proved to be a robust method for extracting texture features from images. Haralick has defined fourteen features from GLCM, for the extraction of the image texture characteristics. Considering a GLCM of size $N_g \times N_g$ and the description of second-order joint probability function of the image is defined as $P(i,j \mid \delta,\theta)$ where *i,j* represents the times of a certain combination that occur in the image which are separated by a δ distance of pixels with angle θ. All the proposed features are listed below:

- Autocorrelation
  Magnitude of texture's smoothness and roughness

$$\sum_{i=1}^{N_g}\sum_{j=1}^{N_g} p(i,j)ij$$

- Join Average
  Gray level intensity distribution

$$\sum_{i=1}^{N_g}\sum_{j=1}^{N_g} p(i,j)i$$

- Cluster Prominence
  Skewness and asymmetry of GLCM. Higher values imply asymmetry, lower value indicates less variation of mean

$$\sum_{i=1}^{N_g}\sum_{j=1}^{N_g}\left(i+j-\mu_\chi-\mu_y\right)^4 p(i,j)$$

  Where $\mu_\chi = \sum_{i=1}^{N_g} p_x(i)i$ and $\mu_y = \sum_{j=1}^{N_g} p_y(j)j$

- Cluster Shade
  Measure of uniformity and skewness of GLCM

$$\sum_{i=1}^{N_g}\sum_{j=1}^{N_g}\left(i+j-\mu_\chi-\mu_y\right)^3 p(i,j)$$

- Cluster Tendency
  Measure of voxels with similar gray level intensities

$$\sum_{i=1}^{N_g}\sum_{j=1}^{N_g}\left(i+j-\mu_\chi-\mu_y\right)^2 p(i,j)$$

- Contrast
  Local intensity variation

$$\sum_{i=1}^{N_g}\sum_{j=1}^{N_g}(i-j)^2 p(i,j)i$$

- Correlation
  Linear dependency of gray level values to their respective voxels in the GLCM

$$\frac{\sum_{i=1}^{N_g}\sum_{j=1}^{N_g} p(i,j)ij-\mu_\chi\mu_y}{\sigma_\chi(i)\sigma_y(j)}$$

  Where $\sigma_\chi(i)\sigma_y(j)$ = standard deviation of *p* in both axes

- Difference Average
  Relationship among sets with similar intensity and sets with different intensities

$$\sum_{k=0}^{N_g-1} kp_{x-y}(k)$$

- Difference Entropy
  Measure of randomness in neighboring gray level intensities

$$\sum_{k=0}^{N_g-1} p_{x-y}(k) log_2(p_{x-y}(k))$$

- Difference Variance
  Measurement of heterogeneity, taking into account pairs of different intensity levels that vary more from the mean

$$\sum_{k=0}^{N_g-1} (k - DA)^2 p_{x-y}(k)$$

  Where *DA = Difference Average*

- Joint Energy
  Measure of homogenous patterns in an image

$$\sum_{i=1}^{N_g} \sum_{j=1}^{N_g} (p(i,j))^2$$

- Joint Entropy
  Measure of variability in neighborhood intensity values

$$-\sum_{i=1}^{N_g} \sum_{j=1}^{N_g} p(i,j) log_2(p(i,j))$$

- Informational Measure of Correlation 1 and 2 (IMC1 & IMC2)
  IMC1 tests the association between the distributions of probabilities where the entropy of x axis is subtracted from the entropy of y axis. IMC2 calculates the same relationship by calculating the logarithmic subtraction of the aforementioned entropies

$$\sum_{i=1}^{N_g}\sum_{j=1}^{N_g} p(i,j)log_2(\frac{p(i,j)}{p_x(i)p_y(j)}) \quad = IMC_1$$

$$\sqrt{1-e^{-2(-IMC_1)}} = IMC_2$$

- Maximal Correlation Coefficient
  Measures the complexity of texture

$$\sqrt{\sum_{k=0}^{N_g}\frac{p(i,k)p(j,k)}{p_x(i)p_y(j)}}$$

While these are the Haralick features, more have been introduced into the GLCM textural features which are mentioned before.

2.2.2. Gray-Level Size-Zone Matrix (GLSZM)

An additional statistical texture descriptor is the Gray-Level Size-Zone Matrix. Similarly to GLCM, GLSZM calculates the pixel intensities of an image. GLSZM considers the relationship between same pixel intensities and areas. While GLCM uses one direction, GLSZM is calculated in all directions. To calculate a GLSZM one has to measure the probabilities of different sized voxels with certain intensities. A simple visualization is shown below:

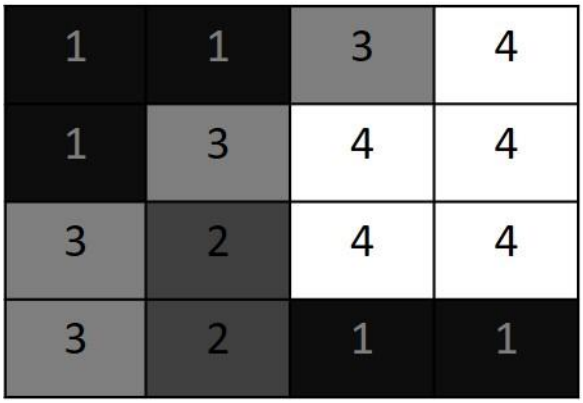

Figure 14: GLSZM example matrix

Considering the above matrix of pixel intensities of an image, the calculation of GLSZM requires to count the size of the relationship between same intensity pixels. The connection which defines a relationship is same intensity value with a pixel offset regardless the direction. A simpler approach/explanation would be to "follow" a single intensity of a pixel and count how many times it occurred in our path.

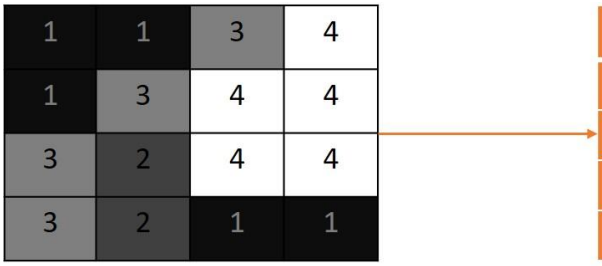

Gray Level / Size zone	1	2	3	4	5
1	0	1	1	0	0
2	0	1	0	0	0
3	0	0	0	1	0
4	0	0	0	0	1

Figure 15: Calculation of the GLSZM of the example matrix

For example, pixels with intensity of 4 value, are connected consisting a zone of the same intensity with size 5. Similarly, for intensity value 3, which occupy a zone of size 4.

GLSZM is particularly effective in characterizing texture homogeneity. Considering that N_g is the number of discreet signal intensities in the image, N_s the number of discreet zones sizes, N_p the number of voxels, $N_z = \sum_{i=1}^{N_g} \sum_{j=1}^{N_s} p(i,j)$ the number of zones and $p(i,j)$ the size zone matrix, the features that can be extracted are listed below:

- Small Area Emphasis
  Measures small area distribution, higher value suggests smaller areas and fine textures
  $$\frac{\sum_{i=1}^{N_g} \sum_{j=1}^{N_s} \frac{p(i,j)}{j^2}}{N_z}$$

- Large Area Emphasis
  Measures the distribution of large size zones, larger values indicate larger size zone and coarse textures
  $$\frac{\sum_{i=1}^{N_g} \sum_{j=1}^{N_s} p(i,j) j^2}{N_z}$$

- Gray Level Non-uniformity (GLN)
  Measures the variance of gray intensity values with a lower value that indicates a greater diversity of intensity values
  $$\frac{\sum_{i=1}^{N_g} \left(\sum_{j=1}^{N_s} p(i,j)\right)^2}{N_z}$$

- Gray Level Non-uniformity Normalized (GLNN)
  Normalized GLN
  $$\frac{\sum_{i=1}^{N_g} \left(\sum_{j=1}^{N_s} p(i,j)\right)^2}{N_z^2}$$

- Size-Zone Non-Uniformity (SZN)
  Measures the diversity of the image size zone volumes with a lower value showing increased homogeneity in the volumes of the size zone
  $$\frac{\sum_{i=1}^{N_s} \left(\sum_{j=1}^{N_g} p(i,j)\right)^2}{N_z}$$

- Size-Zone Non-Uniformity Normalized (SZNN)
  Normalized SZN

$$\frac{\sum_{i=1}^{N_s}\left(\sum_{j=1}^{N_g} p(i,j)\right)^2}{N_z^2}$$

- Zone Percentage
  Measures the texture coarseness by taking the ratio of zones and number of voxels in the ROI

$$\frac{N_z}{N_p}$$

- Gray Level Variance
  Measures the zones' variation of gray level intensity

$$\sum_{i=1}^{N_g}\sum_{j=1}^{N_s} p(i,j)(i-\mu)^2$$

  Where $\mu = \sum_{i=1}^{N_g}\sum_{j=1}^{N_s} p(i,j)i$

- Zone Variance
  Measures the zones' size volume variations

$$\sum_{i=1}^{N_g}\sum_{j=1}^{N_s} p(i,j)(j-\mu)^2$$

  Where $\mu = \sum_{i=1}^{N_g}\sum_{j=1}^{N_s} p(i,j)j$

- Zone Entropy
  Measures the randomness in the variation of zone sizes and gray levels with larger values indicating greater heterogeneity in texture patterns

$$\sum_{i=1}^{N_g}\sum_{j=1}^{N_s} p(i,j)log_2(p(i,j))$$

- Low Gray Level Zone Emphasis (LGLZE)
  Measures the dispersion of lower gray-level size zones with grater values suggesting higher proportion of lower gray-level values and size zones

$$\frac{\sum_{i=1}^{N_g}\sum_{j=1}^{N_s}\frac{p(i,j)}{i^2}}{N_z}$$

- High Gray Level Zone Emphasis (HGLZE)
  Measures the dispersion of higher gray-level values with grater values suggesting higher proportion of higher gray-level values and size zones

$$\frac{\sum_{i=1}^{N_g}\sum_{j=1}^{N_s}p(i,j)i^2}{N_z}$$

- Small Area Low Gray Level Emphasis (SALGLE)
  Measures the ratio of the joint allocation of smaller size zones with lower gray-level values

$$\frac{\sum_{i=1}^{N_g}\sum_{j=1}^{N_s}\frac{p(i,j)}{i^2j^2}}{N_z}$$

- Small Area High Gray Level Emphasis (SAHGLE)
  Measures the proportion of the joint allocation of smaller size zones with higher gray-level values

$$\frac{\sum_{i=1}^{N_g}\sum_{j=1}^{N_s}\frac{p(i,j)i^2}{j^2}}{N_z}$$

- Large Area Low Gray Level Emphasis (LALGLE)
  Measures the ratio of the joint allocation of larger size zones with lower gray-level values

$$\frac{\sum_{i=1}^{N_g}\sum_{j=1}^{N_s}\frac{p(i,j)j^2}{i^2}}{N_z}$$

- Large Area High Gray Level Emphasis (LAHGLE)
  Measures the proportion of the joint allocation of larger size zones with higher gray-level values

$$\frac{\sum_{i=1}^{N_g}\sum_{j=1}^{N_s}p(i,j)i^2j^2}{N_z}$$

2.2.3. Gray Level Run Length Matrix (GLRLM)

A Gray Level Run Length Matrix (GLRLM) quantifies gray level runs of consecutive pixels with the same gray level value, which are defined as the number of pixels. In a GLRLM the y axis represents the number of runs of the gray levels and the x axis the occurrences in the image. GLRLM is calculating for a single angle, however, one can calculate for several angles depending on the application. As with the former matrices, more angles can provide better textural information. The calculation of a GLRLM is illustrated below:

1	2	2	4
1	1	4	4
2	3	3	1
4	4	4	4

Figure 16: An exemplary image/matrix.

As we can see in the figure above (fig.7), for the intensity value 1, there are 4 occasions of a Run Length of 1, 1 occasion of Run Length 2, while for the intensity value 4, one occasion of Run Length 4. Thus, GLRLM is calculated as shown in the figure below where the x axis represents the Run Length and the y axis the intensity value:

	1	2	3	4
1	4	1	0	0
2	3	1	0	0
3	2	1	0	0
4	6	4	2	1

Figure 17: Calculated GLRLM of the fig.7 matrix.

One can deduct several textural features from a GLRLM. Considering N_p is the number of voxels in the image, N_r the number of discreet run lengths, $N_r(\Theta)$ the number of run along angle Θ, N_g the number of discreet intensity values and $p(i,j|\theta)$ the run length matrix along an angle. Several features are described briefly in the list below:

- Short Run Emphasis
  Measures the variation of short run lengths with a higher value suggesting shorter run lengths and fine texture

$$\frac{\sum_{i=1}^{N_g}\sum_{j=1}^{N_r}\frac{p(i,j|\theta)}{j^2}}{N_r(\theta)}$$

- Long Run Emphasis
  Measures the variation of long run lengths with a higher value suggesting longer run lengths and more coarse textures

$$\frac{\sum_{i=1}^{N_g}\sum_{j=1}^{N_r}p(i,j|\theta)j^2}{N_r(\theta)}$$

- Gray Level Non-Uniformity (GLN)
  Measures the similarity of gray-level intensity values in the image where a lower value correlates with a higher intensity similarity

$$\frac{\sum_{i=1}^{N_g}(\sum_{j=1}^{N_r}p(i,j|\theta))^2}{N_r(\theta)}$$

- Gray Level Non-Uniformity Normalized (GLNN)
  GLN normalized version

$$\frac{\sum_{i=1}^{N_g}(\sum_{j=1}^{N_r}p(i,j|\theta))^2}{N_r(\theta)^2}$$

- Run Length Non-Uniformity (RLN)
  Measure the similarity of run lengths throughout the image with a lower value showing greater homogeneity between run lengths in the image

$$\frac{\sum_{i=1}^{N_r}(\sum_{j=1}^{N_g}p(i,j|\theta))^2}{N_r(\theta)}$$

- Run Length Non-Uniformity Normalized (RLNN)
  RLN normalized version

$$\frac{\sum_{i=1}^{N_r}\left(\sum_{j=1}^{N_g} p(i,j|\theta)\right)^2}{N_r(\theta)^2}$$

- Run Percentage (RP)
  Measures the texture coarseness considering the number of runs and the number of voxels in the image with greater values suggesting a larger portion of the image consisting of short runs

$$\frac{N_r(\theta)}{N_p}$$

- Gray Level Variance (GLV)
  Measures the runs' variance in gray level intensity

$$\sum_{i=1}^{N_g}\sum_{j=1}^{N_r} p(i,j|\theta)(i-\mu)^2$$

  Where $\mu = \sum_{i=1}^{N_g}\sum_{j=1}^{N_r} p(i,j|\theta)i$

- Run Variance
  Measures the variance in runs for the run lengths

$$\sum_{i=1}^{N_g}\sum_{j=1}^{N_r} p(i,j|\theta)(j-\mu)^2$$

  Where $\mu = \sum_{i=1}^{N_g}\sum_{j=1}^{N_r} p(i,j|\theta)j$

- Run Entropy
  Measures random distribution of run lengths and gray levels with higher values suggesting higher texture pattern heterogeneity

$$-\sum_{i=1}^{N_g}\sum_{j=1}^{N_r} p(i,j|\theta)log_2(p(i,j|\theta))$$

- Low Gray Level Run Emphasis (LGLRE)
  Measures the distribution of low gray-level values, with a higher value suggesting a higher concentration of low gray-level image values

$$\frac{\sum_{i=1}^{N_g}\sum_{j=1}^{N_r}\frac{p(i,j|\theta)}{i^2}}{N_r(\theta)}$$

- High Gray Level Run Emphasis (HGLRE)
  Measures the distribution of higher gray-level values, with a greater value suggesting a higher concentration of high gray-level image values

$$\frac{\sum_{i=1}^{N_g}\sum_{j=1}^{N_r}p(i,j|\theta)i^2}{N_r(\theta)}$$

- Short Run Low Gray Level Emphasis (SRLGLE)
  Measures the joint distribution of shorter run lengths with lower gray-level values.

$$\frac{\sum_{i=1}^{N_g}\sum_{j=1}^{N_r}\frac{p(i,j|\theta)}{i^2j^2}}{N_r(\theta)}$$

- Short Run High Gray Level Emphasis (SRHGLE)
  Measures the joint distribution of shorter run lengths with higher gray-level values

$$\frac{\sum_{i=1}^{N_g}\sum_{j=1}^{N_r}\frac{p(i,j|\theta)i^2}{j^2}}{N_r(\theta)}$$

- Long Run Low Gray Level Emphasis (LRLGLE)
  Measures the joint distribution of long run lengths with lower gray-level values

$$\frac{\sum_{i=1}^{N_g}\sum_{j=1}^{N_r}\frac{p(i,j|\theta)j^2}{i^2}}{N_r(\theta)}$$

- Long Run High Gray Level Emphasis (LRHGLE)
  Measures the joint distribution of long run lengths with higher gray-level values

$$\frac{\sum_{i=1}^{N_g}\sum_{j=1}^{N_r}p(i,j|\theta)i^2j^2}{N_r(\theta)}$$

3. Gabor Filters

Decomposing a signal into its dominant frequency components has been studied a lot in image processing and signal processing. Especially for local texture recognition, one has to localize the filter in both space and spatial frequency. This is where Gabor filters excel by minimizing the spatial frequency uncertainty relation. [89], [90]. Gabor filters were first introduced in 1946 by Dennis Gabor [89] and were extended, by J. Daugman [90] 42 years later, to a 2-D Gabor filter which provides simultaneous optimal resolution in both spatial and frequency domains. Gabor filters' representations of frequency and orientation, is considered by many contemporary vision scientists to be similar of those of the human visual system[91]. Recently, they have been successfully used in numerous applications, such as texture segmentation[92]–[94], edge detection[95], texture analysis, image analysis and compression[90], character recognition[96], [97], fingerprint recognition[98], [99], face recognition[100], [101], target detection, document analysis and fractal dimension management. Most of these applications face a common problem, the design of the Gabor filter or Gabor filter bank with the appropriate parameters.

The general function form of a 2-D Gabor filter family can be specified as:

$$g_{x,y;\lambda,\theta,\psi,\sigma,\gamma} = e^{-\frac{(x'^2+\gamma^2 y'^2)}{2\sigma^2}} e^{\left(i\left(2\pi\frac{x'}{\lambda}+\varphi\right)\right)}$$

Where: $x' = xcos\theta + ysin\theta$

$$y' = -xsin\theta + ycos\theta$$

The *standard deviation σ* of the Gaussian factor defines the scale of the surrounding area of a pixel in which weighted summation takes place. The eccentricity of the Gaussian and the convolution kernel g is determined by the parameter *γ*, referred as *spatial aspect ratio*. It has a limited range of $0.23 < \gamma < 0.92$.[102]

The parameter λ is the *wavelength* of the sinusoidal factor and $\frac{1}{\lambda}$ the spatial frequency of the harmonic factor. The ratio $\frac{\sigma}{\lambda}$ determines spatial frequency bandwidth of the Gabor Filters. The half-response spatial frequency bandwidth b (in octaves) and the ratio $\frac{\sigma}{\lambda}$ are related as follows:

$$b = \log_2 \frac{\frac{\sigma}{\lambda}\pi + \sqrt{\frac{ln2}{2}}}{\frac{\sigma}{\lambda}\pi - \sqrt{\frac{ln2}{2}}} \ , \frac{\sigma}{\lambda} = \frac{1}{\pi} \sqrt{\frac{ln2}{2}} \cdot \frac{2^b+1}{2^b-1}$$

The *orientation* parameter θ specifies the orientation of the Gabor function. Its value belongs in the interval $[0°, 360°]$. However, values in the interval $[0°, 180°]$ are taken, due to symmetry, the other directions become redundant.[103]

Finally, parameter Φ, which is the *phase offset* of the harmonic factor, determines the symmetry of the function of the Gabor filter.

3.1. Gabor Filter Bank Parameter selection

A sole Gabor filter will be able to identify a pattern of a single orientation and frequency, but to be able to distinguish sophisticated texture patters one must acquire all orientations and frequencies.

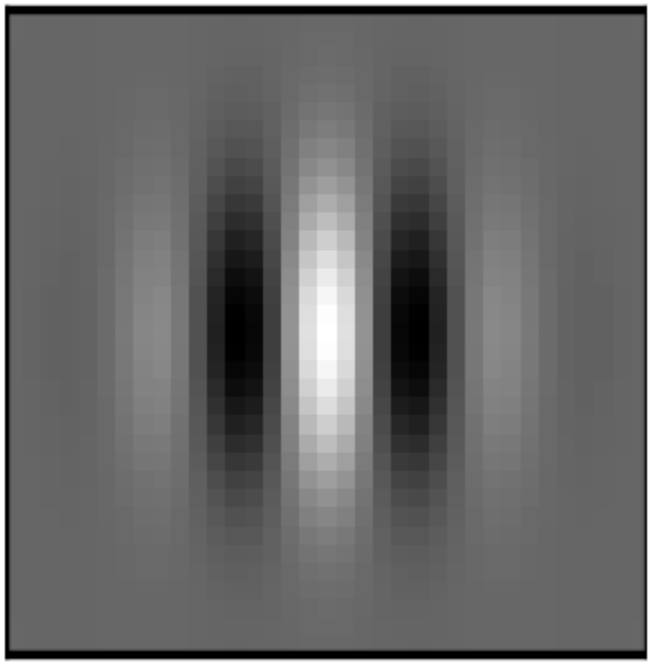

Figure 18: A single Gabor Filter kernel set at orientation = 0π and scale = 0.1

Thus, a Gabor filter bank needs to be created. It includes several of the aforementioned parameters, as vectors, which are adjusted to identify patterns of different frequencies and orientations. This provides us multiple Gabor filters that can detect all possible texture patterns. The design of a Gabor filter bank is dependent on the application that it is used for. However, researchers mostly use similar parameters since they provide sufficient results. As shown in the table below (table 2), the number of orientations vary between 3 and 8 with the most favorable ones being 4 and 8, while the number of scales vary between 3 and 8, the distribution of the values is almost similar. Regarding the selection of the orientation, 4 orientations were selected (figure 9) starting from 0π to 3π/4 with a step of π/4 due to the fact that these orientations cover the most important angles of the image.

Orientations/ Directions	Scales/ Frequencies	Maximum Scale	Scale ratio	Standard Deviation	Wavelength	Authors
$\boldsymbol{\theta_m = \frac{m\pi}{M}}$, $\boldsymbol{M = 8}$	*4(n)*	$\frac{3\pi}{4 \cdot 2^{n-1}}$	*1*	$c_1 = 3$, $c_2 = 5.093$	-	Zheng et al.
8	*5(n)*	*π/4*	$\sqrt{2^n}$	-	$3 \cdot 10^{-6}$	*Lades et al.*
8	*3(n)*	*π/4*	$\sqrt{2^n}$	*π/0.25*	-	*Hen et al.*
8	*8(n)*	*π/4*	$\sqrt{2^n}$	*2π*	-	*Wang et al.*
4	*6*	*1/40*	$\sqrt{3}$	*1*	-	*Ilonen et al.*
8	*5*	*1/4π*	*2*	*2π*	-	*Jahanbin et al.*
8	*3*	*0.56*	*1/5.47*	*0.5*	*0.89*	*Kruizinga et al.*
4	*4*	$\sqrt{2}/4$	$\sqrt{2}/16$	*π/4*	-	*Clausi et al.*
6	*4*	*0.49*	*0.01*	*10*	-	*Mirzapour et al.*
-	*6*	*π*	*π/6*	-	-	*Hammouda*
3	*6*	*0.8*	*0.01*			*Imani et al.*
8	*5*	*2π*	$\sqrt{2}$	*[2.4π, 2.5π… 3π]*	-	*Heng-Chao et al.*
8	*3*	*π/4*	*π/2*	*2*	-	*Yi tou et al.*
3	*3*	*2*	$\sqrt{2}$	*[0.5, 1, 1.5]*		*Bianconni et al.*
6	*6*	*0.5, 0.04(minimum)*	-	-	-	*Shutao Li, Shawe-Taylor*

Table 2: Gabor parameters selected in literature

Concerning scales selection, as aforementioned, we want to explore the multi-scale representation of Gabor filtering and investigate its power on increasing the predictability of the NAC outcome on patients. For that reason, while most of the researches use scales in the range of [0.01, …, 0.5], we chose [0.1, 0.2, 0.3, 0.4, 0.5, 0.6, 0.7, 0.8, 0.9, 1] due to the fact that our regions of interests were small in size, thus requiring larger scale to capture detailed textural information. Additionally, the phase offset was set to 0 (φ=0) and the parameters σ_χ, σ_y were selected to be equal in order to have a circular Gaussian with similar extent in both directions [104]. The standard deviations were not set directly but they were calculated through the wavelength λ and were chosen as: $\sigma_\chi = \sigma_y = 0.56\ \lambda$ which is the result of setting the half-response spatial frequency bandwidth equal to 1 [72].

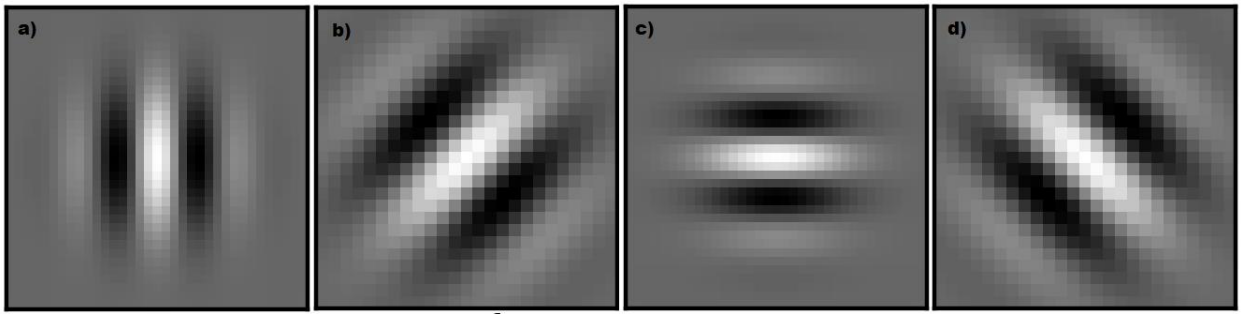

Figure 19: Display of the selected four orientations at scale 0.1. a) is set at 0π, b) is set at π/4, c) is set at π/2 and d) is set at 3π/4

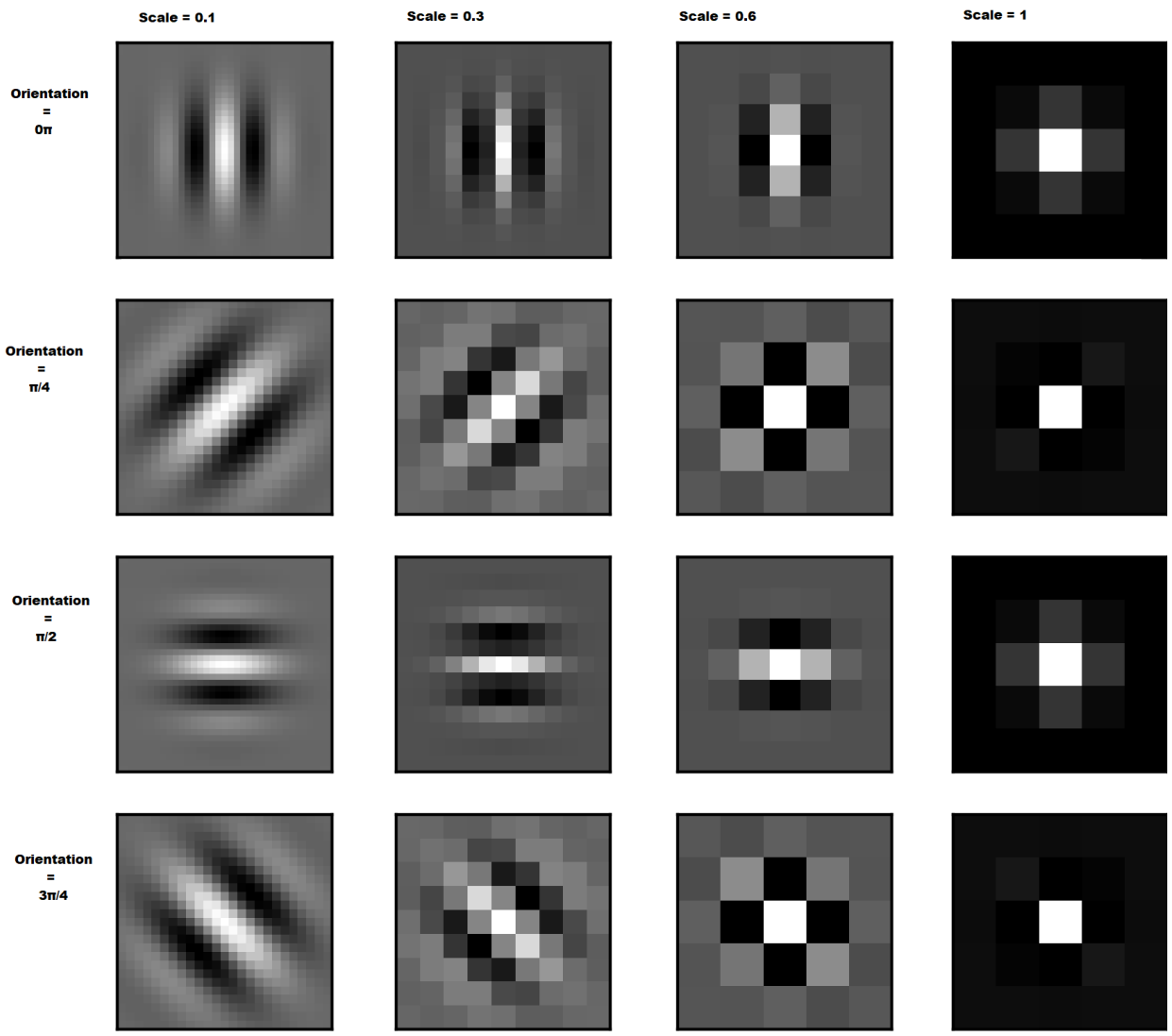

Figure 20: Samples of the Gabor Filter Bank kernels. Shown orientations are: 0π, π/2, π/4 and 3π/4. Shown scales are: 0.1, 0.3, 0.6 and 1

In our study, using the mentioned parameters, we applied 40 Gabor kernels (Gabor filter bank) to each end-phase DCE-MRI exam. As shown in the figure below (Figure 12), we can visually understand the reason for selecting larger scales, since the size of our ROIs is small, smaller scales provide us with a coarse texture response while larger provide adequate textural information. For each Gabor scale-orientation image representation radiomics feature extraction was performed followed by machine learning predictive model analysis (discussed below).

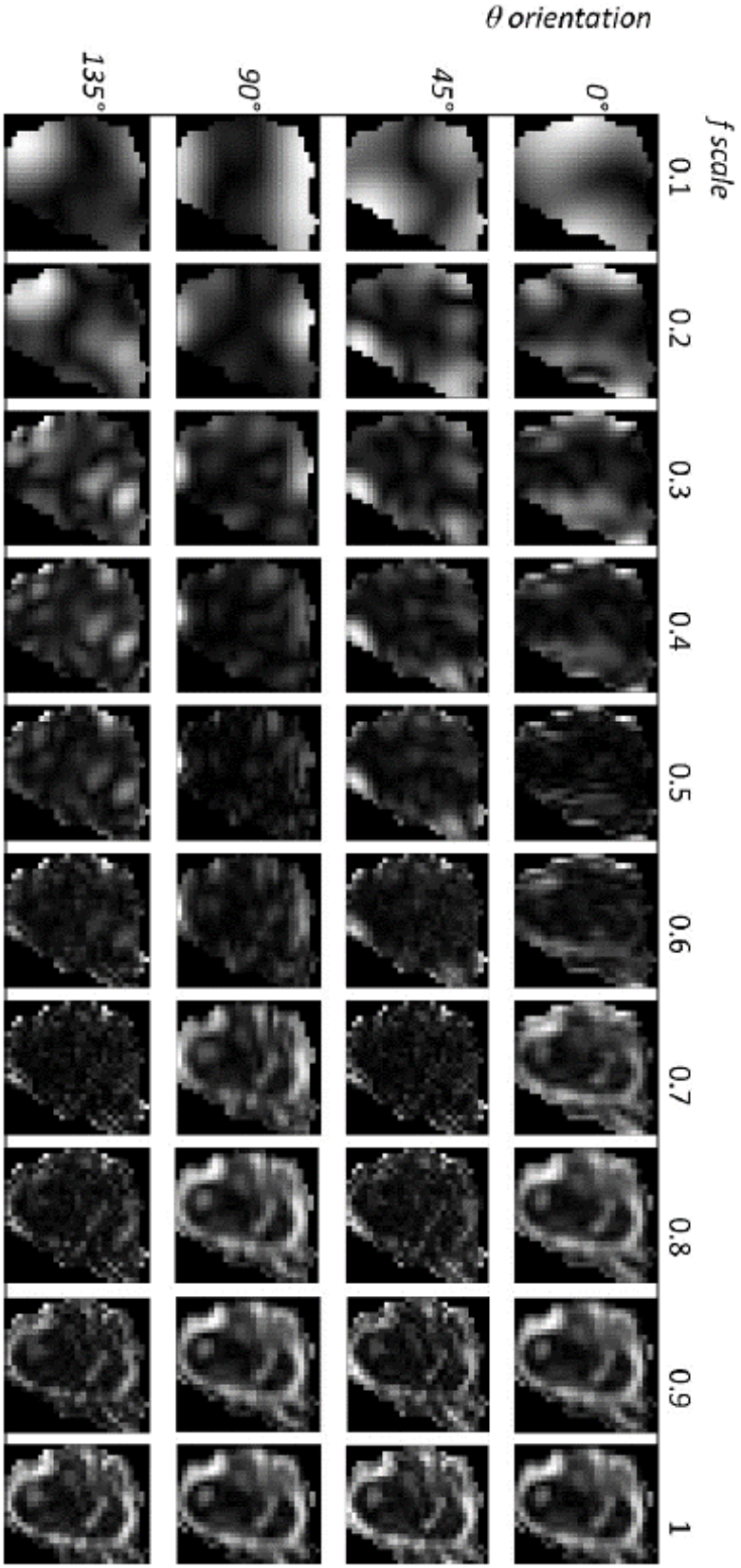

Figure 21: Gabor filter bank applied to a DCE-MRI exam, results are illustrated for the annotated parameter selection. Orientations are {0°, 45°, 90°, 135°} and scales are {0.1, 0.2, 0.3, 0.4, 0.5, 0.6, 0.7, 0.8, 0.9, 1}

4. Results

As mentioned, this thesis contributed to a project focusing on predicting NAC outcome using textural features as predictive factors. The work in this thesis contributed in two conference papers, the first one concerned the predictive strength of radiomic features while the second investigated the predictive strength of multi-scale texture features.

In the first publication regarding texture kinetics, subsequent statistical analysis from co-workers, estimated the predictive strength of the extracted features. This statistical analysis found that 57 features stemming from the four different image sets demonstrated statistical significance (p-value<0.05). In particular, from the baseline exam there were 18 features while from the first follow-up early in the NAC cycle, 39 features. Each feature was calculated in 4 time points of the DCE-MRI: pre-contrast (TP1), peak enhancement (TP2), end-phase (TP3) and difference image between the peak enhancement and the pre-contrast (TP4 = TP2-TP1). Regarding the different image sets, 10 statistically significant features were found on the first (TP1) image-set, 14 from the difference image-set (TP4), 23 from the peak enhancement image set and lastly, 10 features from the end-phase (TP3) as shown in table 3.

Table 3: Number of significant Radiomic Features Per Exam and Image-Set

NAC Exam – DCE-MRI time point	Number of radiomic features
baseline_TP1	5.26% (3/57)
baseline_TP4	8.77% (5/57)
baseline_TP2	7.02% (4/67)
baseline_TP3	10.53% (6/57)
1st follow-up_TP1	12.28% (7/57)
1st follow-up_TP4	15.79% (9/57)
1st follow-up_TP2	33.33% (19/57)
1st follow-up_TP3	7.02% (4/57)

The 8th time point provided the best features for prediction, thanks to the increased contrast of the malignant areas due to the peak enhancement of the contrast agent. Additionally, size-zone non-uniformity normalized feature from the wavelet decomposition of level 2 of the first follow-up using the subtraction image-set (TP4) demonstrated the best predictive performance in the first follow-up NAC exam with AUROC 81.34%. Moreover, about the prediction of outcome at baseline (before therapy administration), the median of the first order statistics from the wavelet decomposition of level 2 end-phase time point image-set, revealed the best predictive ability with AUROC of 80.80%.

In the second publication, both Gabor filtered images and raw images were used to extract radiomic features.[105] However, members of our team conducted a statistical analysis and found that raw-image derived radiomics were not significant in terms of therapy prediction. On the other hand, it was revealed that Gabor filtered derived radiomics were important assets of the classifier used. The XGBoost selected classifiers using the Gabor filtered data, orientations 45° and 90° proved to be persistent among several scale values. More specifically, classifiers of orientation 45° and scale 0.5, orientation 90° and scale 0.7, and orientation 90° and scale 0.9 achieved the highest agreement among all the examined classifiers in terms of the predictive power of features. A visual representation of the relative importance of all radiomic features across the selected classifiers is illustrated in the heatmap below (Figure 14).

The top bar of the figure is related to the feature class (1st order, GLCM, GLRLM and GLSZM) of the radiomic features. Likewise, all selected models were grouped according to their Gabor orientation. Feature importance was scaled from 0 to 100 for comparative purposes. It is visible that different groups of features play important roles in different scale-orientations. Among the most important radiomic features, 3 out of 4 are GLSZM based features which aim to quantify gray level zones in an image. Kurtosis belongs to 1st order statistics, characterize the sharpness of the histogram resulting from the signal intensities of the image.

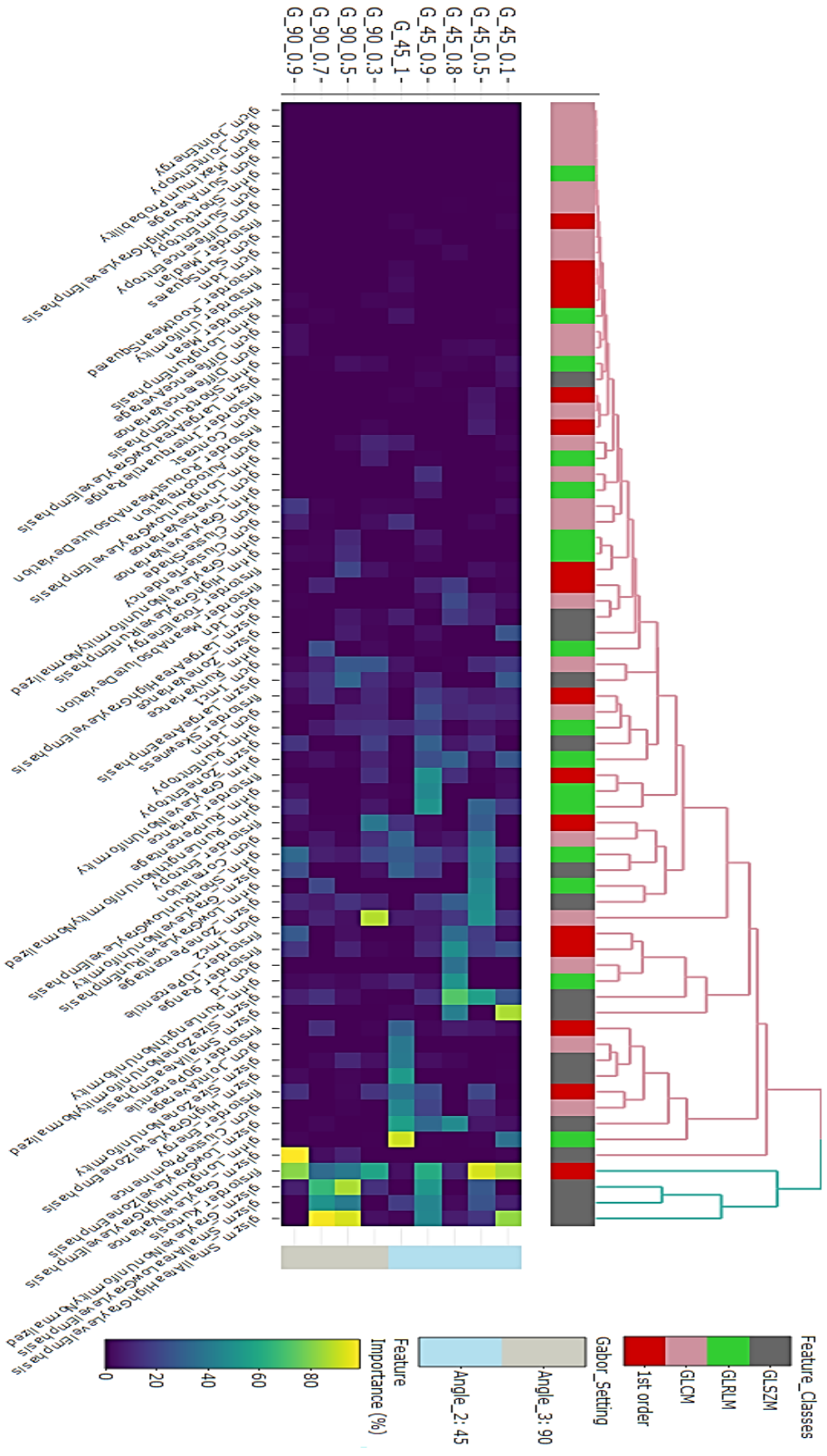

Figure 22: Heatmap and column-based hierarchical clustering describing the relative feature significance of all examined radiomic features during training (columns) and selected classifiers according to thresholding criterion (rows).

5. Discussion

In this study, QIN-Breast public dataset was used for investigating the predictive strength of radiomic features from raw and Gabor filtered images. QIN-Breast was consisted of 35 breast cancer patients receiving NAC treatment with stage II/II providing us with baseline exam data and 1st follow-up exam. In order to examine the predictive precision of radiomic features, four different time points were used, the pre-contrast (TP1), peak enhancement (TP2), the end phase which represents the steady state of the contrast uptake (TP3) and the difference of the 1st time point from the 8th time point (TP2) as a denoting of the pure contrast enhancement (TP4). Results from our first publication revealed that NAC treatment response can be predicted in both baseline and early in the NAC cycle (1st follow-up), with the best predictor features being the median and the size-zone non-uniformity normalized (SZNN) extracted from the wavelet decomposition of level 2 of the baseline and the 1st follow-up exam, achieving an AUROC of 80.80% and 81.34% respectively. In a similar research of Wu et al. [106], based on texture analysis on the same dataset, the most significant result of their multivariate analysis was AUROC = 79%, comparatively our method showed a slight increase on the first follow-up AUROC = 81.34%. Our approach completes an extensive investigation in a large number of texture radiomic features extracted at different DCE-MRI time points whilst taking into account the whole tumor image region.

It is notable from our results that prediction of NAC outcome before the first cycle is possible. Prediction of NAC outcome early in the treatment (after the first cycle) has been investigated to a great extend [107], [108], however, prediction on the baseline exam is still under investigation. Additionally, it is crucial to predict since it could help clinicians on decision making along with optimizing the treatment plan. Several studies have reported that morphological, functional and clinical features are able to distinguish responders from non-responders before the start of NAC treatment [109], [110]. Regardless, these researches were performed on heterogenous data and are not yet established [111]. For this reason, a larger cohort of patients is required to confirm the predictive ability of the baseline exam texture features.

The limitation faced in this research was the small cohort of patients used, as well as being biased in terms of the number of the responders versus non-responders (12 pCR vs 23 non-pCR). Nonetheless, some interesting findings stemmed from this study. Radiomic features proved to have strong predictive abilities and potential and help with understanding tumors architecture. In any case, to establish their clinical significance, more extended studies must be conducted.

The second study emanating from this thesis work investigated the role of Gabor scale-orientation filtering in radiomics-based prediction of NAC therapy. Extreme gradient boosting (XGBoost) was selected to classify DCE-MRI data from the baseline exam and the end-phase time point of the exam. A total of 41 datasets were created consisted of the original image data and their Gabor representation using four orientations {0°, 45°, 90°, 135°} and ten scales {0.1, 0.2, 0.3, 0.4, 0.5, 0.6, 0.7, 0.8, 0.9, 1} for each orientation. A radiomics analysis framework was implemented and 71 features were calculated from 4 distinct feature classes (1st order statistics, GLCM, GLRLM

and GLSZM) for each dataset. Results from the statistical analysis our findings indicated that 9 out of 41 image representations achieved a moderate or good score. All these datasets were based on Gabor-filtered image data generated solely from 45° and 90° of orientation while varying in scale (0.1 to 1). Although maximizing the predictive performance was not the main scope of the current study, all the selected models showed a balanced accuracy above 70%. These results are in line with other recent studies [77], [112], reconfirming the feasibility of baseline prediction of NAC treatment with radiomic features, helping clinicians move towards personalized treatments. From the statistical analysis using XGBoost, four texture features had the highest feature importance when trained, while kurtosis had the overall best performance across scale and orientation having average to high feature importance in most of the selected models.

Ultimately, our results suggest that the proposed Gabor multi-scale orientation methodology can add value in breast cancer therapy prediction. Using this technique, one can explore the scale-orientation persistence of candidate, predictive biomarkers and our results reconfirm that clinically significant texture information exists at different scale while important radiomic features persist in most of the best performing scale-orientation predictive models.

Considering these results and observations, further research on breast cancer therapy prediction can be assisted using multi-scale texture analysis contributing to more personalized treatment decision support tools. Future work can investigate the use of other wavelet decomposition schemes for computing multi-scale texture features. Another suggestion for further work is to use the Gabor filtered extracted features in conjunction with an artificial neural network or deep learning algorithm for the prediction of NAC since such techniques have already proved their importance in many relevant research fields and applications.

6. Bibliography

[1] A. Weiss *et al.*, "Validation Study of the American Joint Committee on Cancer Eighth Edition Prognostic Stage Compared With the Anatomic Stage in Breast Cancer," *JAMA Oncol.*, vol. 4, no. 2, pp. 203–209, Feb. 2018.

[2] C. S. Giess, E. P. Frost, and R. L. Birdwell, "Interpreting one-view mammographic findings: Minimizing callbacks while maximizing cancer detection," *Radiographics*, vol. 34, no. 4, pp. 928–940, 2014.

[3] M. D. Schnall *et al.*, "Diagnostic architectural and dynamic features at breast MR imaging: Multicenter study," *Radiology*, vol. 238, no. 1, pp. 42–53, 2006.

[4] R. LEBORGNE, "Diagnosis of tumors of the breast by simple roentgenography; calcifications in carcinomas.," *Am. J. Roentgenol. Radium Ther. Nucl. Med.*, vol. 65, no. 1, pp. 1–11, Jan. 1951.

[5] L. E. Antonuk *et al.*, "Demonstration of megavoltage and diagnostic x-ray imaging with hydrogenated amorphous silicon arrays," *Med. Phys.*, vol. 19, no. 6, pp. 1455–1466, Nov. 1992.

[6] A. K. Bloomquist, M. J. Yaffe, G. E. Mawdsley, D. M. Hunter, and D. J. Beideck, "Lag and ghosting in a clinical flat-panel selenium digital mammography system," *Med. Phys.*, vol. 33, no. 8, pp. 2998–3005, Jul. 2006.

[7] A. J. Abdelwahab Yousef, "Male Breast Cancer: Epidemiology and Risk Factors," *Semin. Oncol.*, vol. 44, no. 4, pp. 267–272, 2017.

[8] C. Li, H. Zhao, B. Anderson, and H. Jiang, "Multispectral breast imaging using a ten-wavelength, 64×64 source/detector channels silicon photodiode-based diffuse optical tomography system," *Med. Phys.*, vol. 33, no. 3, pp. 627–636, 2006.

[9] P. M. Meaney *et al.*, "Initial Clinical Experience with Microwave Breast Imaging in Women with Normal Mammography," *Acad. Radiol.*, vol. 14, no. 2, pp. 207–218, Feb. 2007.

[10] M. Lazebnik *et al.*, "A large-scale study of the ultrawideband microwave dielectric properties of normal, benign and malignant breast tissues obtained from cancer surgeries," *Phys. Med. Biol.*, vol. 52, no. 20, pp. 6093–6115, Oct. 2007.

[11] R. M. Nishikawa, G. E. Mawdsley, A. Fenster, and M. J. Yaffe, "Scanned projection digital mammography," *Med. Phys.*, vol. 14, no. 5, pp. 717–727, 1987.

[12] M. J. M. Broeders *et al.*, "The impact of mammography screening programmes on incidence

of advanced breast cancer in Europe: a literature review," *BMC Cancer*, vol. 18, no. 1, p. 860, Dec. 2018.

[13] T. Watanabe *et al.*, "Ultrasound Image Classification of Ductal Carcinoma In Situ (DCIS) of the Breast: Analysis of 705 DCIS Lesions," *Ultrasound Med. Biol.*, vol. 43, no. 5, pp. 918–925, May 2017.

[14] P. H. Lento and S. Primack, "Advances and utility of diagnostic ultrasound in musculoskeletal medicine," *Current Reviews in Musculoskeletal Medicine*, vol. 1, no. 1. Humana Press Inc., pp. 24–31, 2008.

[15] K. Schelfout *et al.*, "Contrast-enhanced MR imaging of breast lesions and effect on treatment," *Eur. J. Surg. Oncol.*, vol. 30, no. 5, pp. 501–507, 2004.

[16] P. Mansfield, P. G. Morris, R. Ordidge, R. E. Coupland, H. M. Bishop, and R. W. Blamey, "Carcinoma of the breast imaged by nuclear magnetic resonance (NMR)," *Br. J. Radiol.*, vol. 52, no. 615, pp. 242–243, 1979.

[17] P. C. Lauterbur, "Image formation by induced local interactions: Examples employing nuclear magnetic resonance," *Nature*, vol. 242, no. 5394, pp. 190–191, 1973.

[18] R. M. Mann, N. Cho, and L. Moy, "Breast MRI: State of the Art," *Radiology*, vol. 292, no. 3, pp. 520–536, Sep. 2019.

[19] M. A. Lindquist, "The Statistical Analysis of fMRI Data," *Stat. Sci.*, vol. 23, no. 4, pp. 439–464, Nov. 2008.

[20] L. M. Sherwood, E. E. Parris, and J. Folkman, "Tumor Angiogenesis: Therapeutic Implications," *New England Journal of Medicine*, vol. 285, no. 21. pp. 1182–1186, 18-Nov-1971.

[21] M. Toi, K. Inada, H. Suzuki, and T. Tominaga, "Tumor angiogenesis in breast cancer: Its importance as a prognostic indicator and the association with vascular endothelial growth factor expression," *Breast Cancer Res. Treat.*, vol. 36, no. 2, pp. 193–204, Jan. 1995.

[22] F. J. Gilbert and T. S. Ahearn, "Dynamic contrast-enhanced MRI in cancer," *Imaging Med.*, vol. 1, no. 2, pp. 173–186, 2009.

[23] C. F. G. C. Geraldes and S. Laurent, "Classification and basic properties of contrast agents for magnetic resonance imaging," *Contrast Media and Molecular Imaging*, vol. 4, no. 1. pp. 1–23, 2009.

[24] R. J. De Berardinis and N. S. Chandel, "Fundamentals of cancer metabolism," *Science Advances*, vol. 2, no. 5. American Association for the Advancement of Science, 01-May-2016.

[25] P. J. Kenney, W. T. Sobol, J. K. Smith, and D. E. Morgan, "Computed model of gadolinium enhanced MRI of breast disease," *Eur. J. Radiol.*, vol. 24, no. 2, pp. 109–119, Feb. 1997.

[26] C. K. Kuhl, H. H. Schild, and N. Morakkabati, "Dynamic bilateral contrast-enhanced MR imaging of the breast: Trade-off between spatial and temporal resolution," *Radiology*, vol. 236, no. 3, pp. 789–800, 2005.

[27] D. G. Mitchell, "MR imaging contrast agents - What's in a name?," *Journal of Magnetic Resonance Imaging*, vol. 7, no. 1. pp. 1–4, Jan-1997.

[28] C. K. Kuhl *et al.*, "Dynamic Breast MR Imaging: Are Signal Intensity Time Course Data Useful for Differential Diagnosis of Enhancing Lesions?," *Radiology*, vol. 211, no. 1, pp. 101–110, Apr. 1999.

[29] C. K. Kuhl *et al.*, "Breast MR imaging screening in 192 women proved or suspected to be carrier of a breast cancer susceptibility gene: Preliminary results," *Radiology*, vol. 215, no. 1, pp. 267–279, 2000.

[30] J. Klein *et al.*, "Locally advanced breast cancer treated with neoadjuvant chemotherapy and adjuvant radiotherapy: a retrospective cohort analysis," *BMC Cancer*, vol. 19, no. 1, p. 306, Dec. 2019.

[31] A. G. Waks and E. P. Winer, "Breast Cancer Treatment: A Review," *JAMA - J. Am. Med. Assoc.*, vol. 321, no. 3, pp. 288–300, 2019.

[32] C. Hayes, A. R. Padhani, and M. O. Leach, "Assessing changes in tumour vascular function using dynamic contrast-enhanced magnetic resonance imaging," *NMR Biomed.*, vol. 15, no. 2, pp. 154–163, 2002.

[33] Y. C. Chang, C. S. Huang, Y. J. Liu, J. H. Chen, Y. S. Lu, and W. Y. I. Tseng, "Angiogenic response of locally advanced breast cancer to neoadjuvant chemotherapy evaluated with parametric histogram from dynamic contrast-enhanced MRI," *Phys. Med. Biol.*, vol. 49, no. 16, pp. 3593–3602, Aug. 2004.

[34] M. L. W. Ah-See *et al.*, "Early changes in functional dynamic magnetic resonance imaging predict for pathologic response to neoadjuvant chemotherapy in primary breast cancer," *Clin. Cancer Res.*, vol. 14, no. 20, pp. 6580–6589, Oct. 2008.

[35] L. Martincich *et al.*, "Monitoring response to primary chemotherapy in breast cancer using dynamic contrast-enhanced magnetic resonance imaging," *Breast Cancer Res. Treat.*, vol. 83, no. 1, pp. 67–76, Jan. 2004.

[36] M. D. Pickles, M. Lowry, D. J. Manton, P. Gibbs, and L. W. Turnbull, "Role of dynamic contrast enhanced MRI in monitoring early response of locally advanced breast cancer to neoadjuvant chemotherapy," *Breast Cancer Res. Treat.*, vol. 91, no. 1, pp. 1–10, May 2005.

[37] N. Hylton, "Dynamic contrast-enhanced magnetic resonance imaging as an imaging biomarker.," *J. Clin. Oncol.*, vol. 24, no. 20, pp. 3293–8, Jul. 2006.

[38] J. Caughran *et al.*, "The Effect of the 2009 USPSTF breast cancer screening recommendations on breast cancer in Michigan: A longitudinal study," *Breast J.*, vol. 24, no. 5, pp. 730–737, Sep. 2018.

[39] H. Joshi and M. F. Press, "Molecular oncology of breast cancer," in *The Breast: Comprehensive Management of Benign and Malignant Diseases*, Elsevier Inc., 2018, pp. 282-307.e5.

[40] C. Correa *et al.*, "Accelerated Partial Breast Irradiation: Executive summary for the update of an ASTRO Evidence-Based Consensus Statement," *Pract. Radiat. Oncol.*, vol. 7, no. 2, pp. 73–79, Mar. 2017.

[41] H. Bartelink *et al.*, "Impact of a higher radiation dose on local control and survival in breast-conserving therapy of early breast cancer: 10-year results of the randomized boost versus no boost EORTC 22881-10882 trial.," *J. Clin. Oncol.*, vol. 25, no. 22, pp. 3259–65, Aug. 2007.

[42] T. J. Whelan *et al.*, "Long-Term Results of Hypofractionated Radiation Therapy for Breast Cancer," *N. Engl. J. Med.*, vol. 362, no. 6, pp. 513–520, Feb. 2010.

[43] I. H. Kunkler, L. J. Williams, W. J. L. Jack, D. A. Cameron, and J. M. Dixon, "Breast-conserving surgery with or without irradiation in women aged 65 years or older with early breast cancer (PRIME II): A randomised controlled trial," *Lancet Oncol.*, vol. 16, no. 3, pp. 266–273, Mar. 2015.

[44] T. J. Whelan *et al.*, "Regional nodal irradiation in early-stage breast cancer," *N. Engl. J. Med.*, vol. 373, no. 4, pp. 307–316, 2015.

[45] T. J. Whelan *et al.*, "Regional Nodal Irradiation in Early-Stage Breast Cancer," *N. Engl. J. Med.*, vol. 373, no. 4, pp. 307–316, Jul. 2015.

[46] D. N. Krag *et al.*, "Technical outcomes of sentinel-lymph-node resection and conventional axillary-lymph-node dissection in patients with clinically node-negative breast cancer: results from the NSABP B-32 randomised phase III trial," *Lancet Oncol.*, vol. 8, no. 10, pp. 881–888, 2007.

[47] B. Fisher *et al.*, "Twenty-Year Follow-up of a Randomized Trial Comparing Total Mastectomy, Lumpectomy, and Lumpectomy plus Irradiation for the Treatment of Invasive Breast Cancer," *N. Engl. J. Med.*, vol. 347, no. 16, pp. 1233–1241, Oct. 2002.

[48] D. N. Krag *et al.*, "Sentinel-lymph-node resection compared with conventional axillary-lymph-node dissection in clinically node-negative patients with breast cancer: Overall survival findings from the NSABP B-32 randomised phase 3 trial," *Lancet Oncol.*, vol. 11,

no. 10, pp. 927–933, Oct. 2010.

[49] M. L. Citron *et al.*, "Randomized trial of dose-dense versus conventionally scheduled and sequential versus concurrent combination chemotherapy as postoperative adjuvant treatment of node-positive primary breast cancer: first report of Intergroup Trial C9741/Cancer and Leukemia Group B Trial 9741.," *J. Clin. Oncol.*, vol. 21, no. 8, pp. 1431–9, Apr. 2003.

[50] S. Darby *et al.*, "Effect of radiotherapy after breast-conserving surgery on 10-year recurrence and 15-year breast cancer death: Meta-analysis of individual patient data for 10 801 women in 17 randomised trials," *Lancet*, vol. 378, no. 9804, pp. 1707–1716, 2011.

[51] K. Clark *et al.*, "The cancer imaging archive (TCIA): Maintaining and operating a public information repository," *J. Digit. Imaging*, vol. 26, no. 6, pp. 1045–1057, 2013.

[52] M. Kaufmann *et al.*, "International expert panel on the use of primary (preoperative) systemic treatment of operable breast cancer: Review and recommendations," *Journal of Clinical Oncology*, vol. 21, no. 13. pp. 2600–2608, 01-Jul-2003.

[53] G. M. Kiebert, J. C. J. M. De Haes, and C. J. H. Van De Velde, "The impact of breast-conserving treatment and mastectomy on the quality of life of early-stage breast cancer patients: A review," *J. Clin. Oncol.*, vol. 9, no. 6, pp. 1059–1070, Jun. 1991.

[54] J. S. D. Mieog, J. A. van der Hage, and C. J. H. van de Velde, "Neoadjuvant chemotherapy for operable breast cancer," *Br. J. Surg.*, vol. 94, no. 10, pp. 1189–1200, Oct. 2007.

[55] G. von Minckwitz *et al.*, "In vivo chemosensitivity-adapted preoperative chemotherapy in patients with early-stage breast cancer: The GEPARTRIO pilot study," *Ann. Oncol.*, vol. 16, no. 1, pp. 56–63, Jan. 2005.

[56] H. D. Bear *et al.*, "Sequential preoperative or postoperative docetaxel added to preoperative doxorubicin plus cyclophosphamide for operable breast cancer: National surgical adjuvant breast and bowel project protocol B-27," *J. Clin. Oncol.*, vol. 24, no. 13, pp. 2019–2027, May 2006.

[57] I. C. Smith *et al.*, "Neoadjuvant chemotherapy in breast cancer: Significantly enhanced response with docetaxel," *J. Clin. Oncol.*, vol. 20, no. 6, pp. 1456–1466, Mar. 2002.

[58] M. L. W. Ah-See *et al.*, "Early changes in functional dynamic magnetic resonance imaging predict for pathologic response to neoadjuvant chemotherapy in primary breast cancer," *Clin. Cancer Res.*, vol. 14, no. 20, pp. 6580–6589, 2008.

[59] S. H. Park *et al.*, "Diffusion-weighted MR imaging: Pretreatment prediction of response to neoadjuvant chemotherapy in patients with breast cancer," *Radiology*, vol. 257, no. 1, pp. 56–63, 2010.

[60] J. Wu *et al.*, "Robust Intratumor Partitioning to Identify High-Risk Subregions in Lung Cancer: A Pilot Study," *Int. J. Radiat. Oncol. Biol. Phys.*, vol. 95, no. 5, pp. 1504–1512, 2016.

[61] A. Ahmed, P. Gibbs, M. Pickles, and L. Turnbull, "Texture analysis in assessment and prediction of chemotherapy response in breast cancer.," *J. Magn. Reson. Imaging*, vol. 38, no. 1, pp. 89–101, Jul. 2013.

[62] S. C. Agner *et al.*, "Textural kinetics: A novel dynamic contrast-enhanced (DCE)-MRI feature for breast lesion classification," *J. Digit. Imaging*, vol. 24, no. 3, pp. 446–463, 2011.

[63] G. Thibault *et al.*, "DCE-MRI Texture Features for Early Prediction of Breast Cancer Therapy Response," *Tomography*, vol. 3, no. 1, pp. 23–32, 2017.

[64] N. Michoux *et al.*, "Texture analysis on MR images helps predicting non-response to NAC in breast cancer," *BMC Cancer*, vol. 15, no. 1, pp. 1–13, 2015.

[65] J. R. Teruel *et al.*, "Dynamic contrast-enhanced MRI texture analysis for pretreatment prediction of clinical and pathological response to neoadjuvant chemotherapy in patients with locally advanced breast cancer," *NMR Biomed.*, vol. 27, no. 8, pp. 887–896, 2014.

[66] M. J. Gangeh, B. M. Ter Haar Romeny, and C. Eswaran, "Scale-space texture classification using combined classifiers," *Lect. Notes Comput. Sci. (including Subser. Lect. Notes Artif. Intell. Lect. Notes Bioinformatics)*, vol. 4522 LNCS, no. January 2015, pp. 324–333, 2007.

[67] S. Andra and Y. Wu, "Multiresolution histograms for SVM-based texture classification," *Lect. Notes Comput. Sci. (including Subser. Lect. Notes Artif. Intell. Lect. Notes Bioinformatics)*, vol. 3656 LNCS, pp. 754–761, 2005.

[68] T. Ojala, M. Pietikainen, and T. Maenpaa, "Multiresolution gray-scale and rotation invariant texture classification with local binary patterns," *IEEE Trans. Pattern Anal. Mach. Intell.*, vol. 24, no. 7, pp. 971–987, 2002.

[69] L. Wang and J. Liu, "Texture classification using multiresolution Markov random field models," *Pattern Recognit. Lett.*, vol. 20, no. 2, pp. 171–182, 1999.

[70] T. Randen and J. H. Husøy, "Filtering for texture classification: A comparative study," *IEEE Trans. Pattern Anal. Mach. Intell.*, vol. 21, no. 4, pp. 291–310, 1999.

[71] S. Li and J. Shawe-Taylor, "Comparison and fusion of multiresolution features for texture classification," *Pattern Recognit. Lett.*, vol. 26, no. 5, pp. 633–638, 2005.

[72] A. K. Jain and F. Farrokhnia, "Unsupervised texture segmentation using Gabor filters," vol. 000, pp. 14–19, 2002.

[73] G. M. Haley and B. S. Manjunath, "Rotation invariant texture classification using a

complete space frequency model," *IEEE Trans. Image Process.*, vol. 8, no. 2, pp. 255–269, 1999.

[74] C. E. Loo *et al.*, "Dynamic contrast-enhanced MRI for prediction of breast cancer response to neoadjuvant chemotherapy: Initial results," *Am. J. Roentgenol.*, vol. 191, no. 5, pp. 1331–1338, Nov. 2008.

[75] R. Johansen *et al.*, "Predicting survival and early clinical response to primary chemotherapy for patients with locally advanced breast cancer using DCE-MRI," *J. Magn. Reson. Imaging*, vol. 29, no. 6, pp. 1300–1307, Jun. 2009.

[76] M. Fan, G. Wu, H. Cheng, J. Zhang, G. Shao, and L. Li, "Radiomic analysis of DCE-MRI for prediction of response to neoadjuvant chemotherapy in breast cancer patients," *Eur. J. Radiol.*, vol. 94, pp. 140–147, 2017.

[77] Z. Liu *et al.*, "Radiomics of multiparametric MRI for pretreatment prediction of pathologic complete response to neoadjuvant chemotherapy in breast cancer: A multicenter study," *Clin. Cancer Res.*, vol. 25, no. 12, pp. 3538–3547, 2019.

[78] X. Li *et al.*, "Multiparametric magnetic resonance imaging for predicting pathological response after the first cycle of neoadjuvant chemotherapy in breast cancer," *Invest. Radiol.*, vol. 50, no. 4, p. 195—204, Apr. 2015.

[79] D. M. Sataloff, B. A. Mason, A. J. Prestipino, U. L. Seinige, C. P. Lieber, and Z. Baloch, "Pathologic response to induction chemotherapy in locally advanced carcinoma of the breast: a determinant of outcome.," *J. Am. Coll. Surg.*, vol. 180, no. 3, pp. 297–306, Mar. 1995.

[80] X. Li *et al.*, "Combined DCE-MRI and DW-MRI for Predicting Breast Cancer Pathological Response After the First Cycle of Neoadjuvant Chemotherapy," *Invest. Radiol.*, vol. 50, no. 4, pp. 195–204, 2015.

[81] R. M. Haralick, K. Shanmugam, and I. Dinstein, "Textural Features for Image Classification," *IEEE Trans. Syst. Man. Cybern.*, vol. SMC-3, no. 6, pp. 610–621, 1973.

[82] I. Hersey and P. Brodatz, "Textures: A Photographic Album for Artists and Designers," *Leonardo*, vol. 1, no. 1, p. 91, Jan. 1968.

[83] W. K. Pratt, O. D. Faugeras, and A. Gagalowicz, "Visual Discrimination of Stochastic Texture Fields," *IEEE Trans. Syst. Man Cybern.*, vol. 8, no. 11, pp. 796–804, 1978.

[84] R. M. Haralick, "Statistical and structural approaches to texture," *Proc. IEEE*, vol. 67, no. 5, pp. 786–804, 1979.

[85] E. Kontopodis *et al.*, "DCE-MRI radiomics features for predicting breast cancer neoadjuvant therapy response," *IST 2018 - IEEE Int. Conf. Imaging Syst. Tech. Proc.*, vol.

3, pp. 1–6, 2018.

[86] J. J. M. Van Griethuysen *et al.*, "Computational radiomics system to decode the radiographic phenotype," *Cancer Res.*, vol. 77, no. 21, pp. e104–e107, 2017.

[87] B. Li and M. Q. H. Meng, "Texture analysis for ulcer detection in capsule endoscopy images," *Image Vis. Comput.*, vol. 27, no. 9, pp. 1336–1342, 2009.

[88] Y. Hu, C. Zhao, and H. Wang, "Directional Analysis of Texture Images Using Gray Level Co-Occurrence Matrix," in *2008 IEEE Pacific-Asia Workshop on Computational Intelligence and Industrial Application*, 2008, vol. 2, pp. 277–281.

[89] D. Gabor, "Theory of communication," *Journal of the Institution of Electrical Engineers - Part I: General*, vol. 94, no. 73. pp. 58–58, 2014.

[90] J. G. Daugman, "Complete Discrete 2-D Gabor Transforms by Neural Networks for Image Analysis and Compression," *IEEE Trans. Acoust.*, vol. 36, no. 7, pp. 1169–1179, 1988.

[91] A. R. Rao and G. L. Lohse, "Identifying High Level Features of Texture Perception," *CVGIP: Graphical Models and Image Processing*, vol. 55, no. 3. pp. 218–233, 1993.

[92] T.~P.~Weldon, W.~E.~Higgins, and D.~F.~Dunn, "Efficient Gabor filter design for texture segmentation," *Pattern Recognit.*, vol. 29, no. 12, pp. 2005–2015, 1996.

[93] C. C. Chen and D. C. Chen, "Multi-resolutional gabor filter in texture analysis," *Pattern Recognit. Lett.*, vol. 17, no. 10, pp. 1069–1076, 1996.

[94] A. Bodnarova, M. Bennamoun, and S. Latham, "Optimal gabor filters for textile flaw detection," *Pattern Recognit.*, vol. 35, no. 12, pp. 2973–2991, 2002.

[95] K. R. Namuduri, R. Mehrotra, and N. Ranganathan, "Edge detection models based on gabor filters," *Proc. - Int. Conf. Pattern Recognit.*, vol. 3, pp. 729–732, 1992.

[96] V. Tavsanoglu and E. Saatci, "Feature extraction for character recognition using Gabor-type filters implemented by cellular neural networks," pp. 63–68, 2002.

[97] Y. M. Su and J. F. Wang, "A novel stroke extraction method for Chinese characters using Gabor filters," *Pattern Recognit.*, vol. 36, no. 3, pp. 635–647, 2003.

[98] J. Yang, L. Liu, T. Jiang, and Y. Fan, "A modified Gabor filter design method for fingerprint image enhancement," *Pattern Recognit. Lett.*, vol. 24, no. 12, pp. 1805–1817, 2003.

[99] Chih-Jen Lee, Sheng-De Wang, and Kuo-Ping Wu, "Fingerprint recognition using principal Gabor basis function," pp. 393–396, 2002.

[100] J. Lampinen and S. Member, "Based on Self-organizing Feature Extraction," vol. 6, no. 3,

1995.

[101] Y. Chen, "Independent component analysis of Gabor features for texture classification," *Opt. Eng.*, vol. 47, no. 12, p. 127003, 2008.

[102] N. Petkov and P. Kruizinga, "Computational models of visual neurons specialised in the detection of periodic and aperiodic oriented visual stimuli: Bar and grating cells," *Biol. Cybern.*, vol. 76, no. 2, pp. 83–96, 1997.

[103] K. Afrin, "Classification and feature extraction of binucleate cells using Mahalanobis distance and Gabor wavelet analysis," *Int. J. Intell. Eng. Informatics*, vol. 2, no. 4, p. 304, 2015.

[104] D. A. Clausi and M. Ed Jernigan, "Designing Gabor filters for optimal texture separability," *Pattern Recognit.*, vol. 33, no. 11, pp. 1835–1849, 2000.

[105] G. C. Manikis *et al.*, "Scale-space DCE-MRI radiomics analysis based on Gabor filters for predicting breast cancer therapy response."

[106] J. Wu, G. Gong, Y. Cui, and R. Li, "Intratumor partitioning and texture analysis of dynamic contrast-enhanced (DCE)-MRI identifies relevant tumor subregions to predict pathological response of breast cancer to neoadjuvant chemotherapy," *J. Magn. Reson. Imaging*, vol. 44, no. 5, pp. 1107–1115, 2016.

[107] S. Ueda *et al.*, "Baseline tumor oxygen saturation correlates with a pathologic complete response in breast cancer patients undergoing neoadjuvant chemotherapy.," *Cancer Res.*, vol. 72, no. 17, pp. 4318–4328, Sep. 2012.

[108] D. Generali *et al.*, "Hypoxia-inducible factor-1alpha expression predicts a poor response to primary chemoendocrine therapy and disease-free survival in primary human breast cancer.," *Clin. Cancer Res.*, vol. 12, no. 15, pp. 4562–4568, Aug. 2006.

[109] T. Uematsu, M. Kasami, and S. Yuen, "Neoadjuvant chemotherapy for breast cancer: Correlation between the baseline MR imaging findings and responses to therapy," *Eur. Radiol.*, vol. 20, no. 10, pp. 2315–2322, 2010.

[110] S. Michishita *et al.*, "Prediction of pathological complete response to neoadjuvant chemotherapy by magnetic resonance imaging in breast cancer patients," *Breast*, vol. 24, no. 2, pp. 159–165, 2015.

[111] R. Prevos *et al.*, "Pre-treatment differences and early response monitoring of neoadjuvant chemotherapy in breast cancer patients using magnetic resonance imaging: A systematic review," *Eur. Radiol.*, vol. 22, no. 12, pp. 2607–2616, 2012.

[112] N. M. Braman *et al.*, "Intratumoral and peritumoral radiomics for the pretreatment prediction of pathological complete response to neoadjuvant chemotherapy based on breast

DCE-MRI," *Breast Cancer Res.*, vol. 19, no. 1, pp. 1–14, 2017.

[113] G. Lee, H. Y. Lee, E. S. Ko, and W. K. Jeong, "Radiomics and imaging genomics in precision medicine," *Precis. Futur. Med.*, vol. 1, no. 1, pp. 10–31, Mar. 2017.